



Article

Feasibility Study of the Seven-Bar Linkage 7-PR(RRRR)RP Used for Medical Disinfection Robot †

Elida-Gabriela Tulcan , Carmen Sticlaru, Alexandru Oarcea , Melania Olivia Sandu, Narcis-Grațian Crăciun and Erwin-Christian Lovasz *

Department of Mechatronics, Politehnica University of Timişoara, 300006 Timişoara, Romania; elida.tulcan@upt.ro (E.-G.T.); carmen.sticlaru@upt.ro (C.S.); alexandru.oarcea@student.upt.ro (A.O.); melania.sandu@upt.ro (M.O.S.); narcis.craciun@student.upt.ro (N.-G.C.)

- * Correspondence: erwin.lovasz@upt.ro
- [†] This article is a revised and extended version of the paper entitled Analytical Synthesis of the Seven-Bar Linkage 7-PR(RRRR)RP used for Medical Disinfection Robot. In Proceedings of the 6th IFToMM Symposium on Mechanism Design for Robotics, Timişoara, Romania, 27–29 June 2024.

Abstract: Current disinfection robots either have a bulky design or cannot operate in multiple configurations, therefore being unable to disinfect the hard-to-reach areas, which leads to low efficiency of the disinfection process. A solution for this problem would be to use disinfection robots with folding mechanisms which can operate in different configurations based on the area type that needs to be disinfected. This paper presents the feasibility study of the 7-PR(RRRR)RP seven-bar linkage used for a disinfection robot with folding mechanism. First, the structure's parameters were computed with a synthesis method by developing the inequalities system in order to avoid the singularities positions of the mechanism. This initial method took into consideration different values of the design coefficient p (which indicates the two possible designs of the selected linkage) and an arbitrary value of the coefficient k > 1, which was imposed in order to substitute the resulting inequalities system with an equation system. However, applying this method does not ensure that the optimal 7-PR(RRRR)RP seven-bar linkage structure for the design of a medical disinfection robot is obtained. Furthermore, an optimized synthesis method was applied, which took into consideration the ratio between the total height of the mechanism and its total size. The parameters of the seven-bar linkage were computed for multiple values of the design coefficient $p \in [1.1; 2]$ and multiple values of the coefficient $k \in (0; 2]$, while a target function was implemented in order to identify the mechanism with the highest height range and the lowest size, which is considered to be the optimal structure for the design of a medical disinfection robot with a folding mechanism. The accuracy and the reliability of the results are furthermore strengthened by a performance analysis between the optimal indicated structure from the optimized synthesis method and other 7-PR(RRRR)RP seven-bar linkage structures, which were computed with different values of the parameters.

Keywords: healthcare; medical robots; disinfection robots; folding mechanisms; seven-bar linkages

check for updates

Citation: Tulcan, E.-G.; Sticlaru, C.; Oarcea, A.; Sandu, M.O.; Crăciun, N.-G.; Lovasz, E.-C. Feasibility Study of the Seven-Bar Linkage 7-PR(RRRR)RP Used for Medical Disinfection Robot. *Robotics* **2024**, *13*, 177. https://doi.org/10.3390/ robotics13120177

Academic Editor: Dan Zhang

Received: 30 October 2024 Revised: 28 November 2024 Accepted: 9 December 2024 Published: 12 December 2024



Copyright: © 2024 by the authors. Licensee MDPI, Basel, Switzerland. This article is an open access article distributed under the terms and conditions of the Creative Commons Attribution (CC BY) license (https://creativecommons.org/licenses/by/4.0/).

1. Introduction

Medical disinfection robots are often used in order to perform air, water, and surface sterilization procedures [1]. They are mainly used in medical areas such as hospitals, laboratories, and clinics, but also in other facilities, such as hotels, offices, and schools. Every disinfection robot use a particular technology in order to perform the sanitation process, each of them with their own advantages and limitations [2]. Most of the current disinfection robots primarily use either pulsed xenon UV lamps or mercury-vapor UV lamps as the disinfection source [3,4]. Other disinfection robots use disinfectant sprays [5–7] such as chlorine compounds or dry mist hydrogen peroxide in order to perform air, water, and surfaces disinfection. In some other cases, they mix both technologies and provide both UV-C and spraying disinfection [8–12]. Table 1 presents the current state of medical

Robotics 2024, 13, 177 2 of 24

disinfection robots in terms of autonomy, environment, size, disinfection method, and disinfection source.

This article is part of a series of papers [13–17] in which different types of planar mechanisms are analyzed in order to establish the most feasible structure for the design of a medical disinfection robot with a folding mechanism. For example, a proposed design for a medical disinfection robot with a four-bar linkage as the folding mechanism's structure [16] has a height of 50.6 mm in the minimum configuration and 232.4 mm in the maximum configuration, while its total size is 591.1 mm, considered very large. Other example of a possible folding mechanism structure is the five-bar linkage [17], which has a height of 130 mm in the minimum configuration and 330 mm in the maximum configuration, while the total size of the mechanism is almost 300 mm.

The seven-bar linkage was considered mostly because it allows a high range of the mechanism's height between its minimum configuration (folded position) and maximum configuration (extended position), while at the same time keeping the overall size small. As already presented [18], disinfection robots which cannot operate in multiple configurations cannot disinfect both large and hard-to-reach areas; therefore, disinfection robots with folding mechanisms should be considered in order to perform the most effective disinfection process possible.

The main objective of this paper is to identify the optimal 7-PR(RRRR)RP seven-bar linkage for the design of a medical disinfection robot with a folding mechanism. First, the parameters of the seven-bar linkage are computed as a result of the initial synthesis method, with an arbitrary coefficient k and for different values of the design coefficient p, which does not guarantee the obtention of the optimal structure for the intended purpose. The optimized synthesis approach takes into consideration the height and the size of the mechanism while it computes the mechanism's parameters for different values of the coefficient k and the design coefficient p. Having said that, the optimal structure should provide the best ratio between the total height (the height range between the minimum configuration, also referred as the folded position, and the maximum configuration, also referred as the extended position), which needs to be as high as possible, and the total size of the mechanism, which needs to be as low as possible. Furthermore, the accuracy and the reliability of the results obtained are strengthened by a performance analysis between the structure which was indicated as optimal from the optimized synthesis method and other structures computed with different parameters.

Table 1. Current state of medical disinfection robots.

Source	Autonomous	Environment	Size (L \times W \times H) [mm]	Disinfection Method	Disinfection Source
[19]	Semi	Hospitals	$760 \times 480 \times 1100$	UV-C Light	6 UV-C Lamps
[20]	No	Hospitals	1100 × 700 × 1800	UV-C Light	8 UV-C Lamps
[21]	No	Medical Facilities	$900\times 665\times 1745$	UV-C Light	8 UV-C Lamps
[22]	Yes	Indoor	$300\times200\times1200$	Spray	Hydrogen Peroxide
[23]	No	Medical Facilities	252 × 252 × 1123	UV-C Light	3 UV-C Lamps
[24]	Yes	Hospitals	930 × 660 × 1710	UV-C Light	8 UV-C Lamps
[25]	No	Indoor	$500 \times 300 \times 640$	UV-C Light	5 UV-C Lamps
[26]	Yes	Indoor	$340\times340\times840$	UV-C Light	3 UV-C Lamps
[27]	Yes	Small Indoor	$435\times390\times415$	UV-C Light	5 UV-C Lamps
[28]	Yes	Indoor	$710\times610\times865$	UV-C Light	1 UV-C Lamp
[29]	No	Indoor	$350\times350\times1500$	UV-C Light	1 UV-C Lamp
[30]	No	Hospitals	$440\times440\times860$	Spray	Chlorine Dioxide
[31]	Yes	Indoor	915 × 915 × 600	UV-C Light	4 UV-C Lamps
[32]	No	Ambulances	$505 \times 500 \times 120$	UV-C Light	1 UV-C Lamp

Robotics 2024, 13, 177 3 of 24

2. Synthesis of the Symmetrical Seven-Bar Linkage

Starting from the condition of having a fully constrained mechanism structure and considering as input conditions the mechanism's degree of freedom (DOF) as M = 2, the number of kinematic loops (N = 2), the number of kinematic pairs (e_1) only with DOF = 1, and the number of elements (n) results the following relationship:

$$e_1 = \frac{3 \cdot n - 5}{2} \in \mathbf{N} \tag{1}$$

The only convenient solution of Equation (1), which is relevant for our study of the seven-bar linkage, is the following:

$$n = 7 \rightarrow e_1 = 8 \tag{2}$$

The number of elements of different ranks result from the Diophantine equation system:

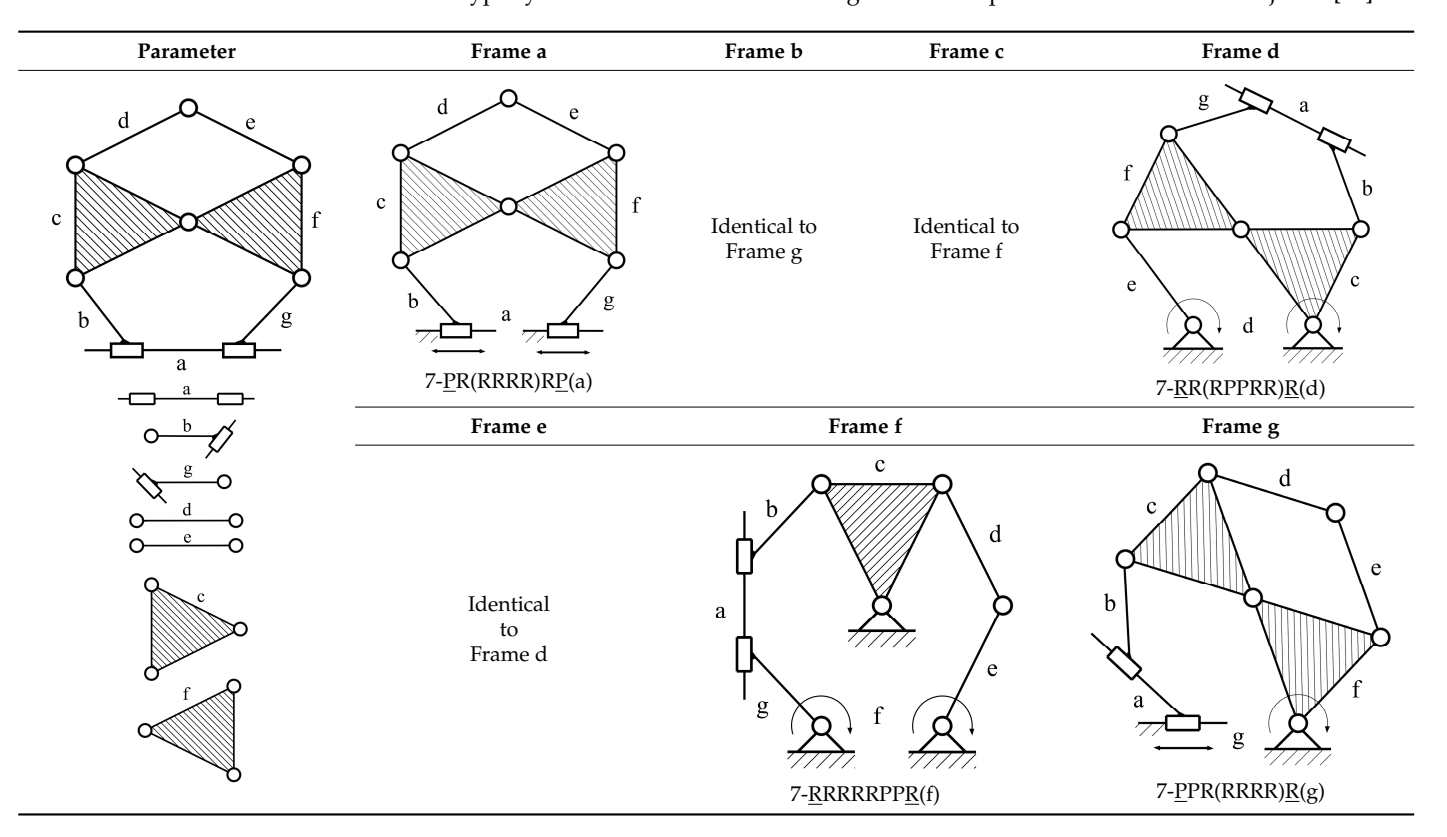
$$\begin{cases}
7 = n_2 + n_3 \\
16 = 2 \cdot n_2 + 3 \cdot n_3
\end{cases}$$
(3)

with the following solution:

$$n_2 = 5$$
(binary elements), $n_3 = 2$ (ternary elements) (4)

By applying the Franz Reuleaux type synthesis method for the kinematic chain of the seven-bar linkage using two prismatic joints and six revolute joints, we obtain the linkage structures presented in Table 2, where the identical structures were removed and are only indicated in the figure as identical to other.

Table 2. Type synthesis of the seven-bar linkages with two prismatic and six revolute joints [15].



This method consists of subsequently considering an element as frame, two elements (jointed in frame) as the drive elements, and either one element as the driven element or one

Robotics 2024, 13, 177 4 of 24

joint as the characteristic point. The notation that will be used for this type of linkage chain is 7-PR(RRRR)RP(a), where R represents the revolute joint and P represents the prismatic joint. Additionally, the underlined letters represent the drive joints, the letters between the first brackets indicate the parallel connected kinematic chain, while the letter between the last brackets indicates the considered frame element (e.g., (a)). The analyzed seven-bar linkage 7-PR(RRRR)RP was chosen from Table 2 because of its symmetrical design on the y axis.

Figures 1 and 2 show the two possible kinematic designs of the selected linkage 7- $\underline{P}R(RRR)R\underline{P}$. The first kinematic design results directly from the type synthesis of the seven-bar linkage with six revolute joints and two prismatic joints. The second kinematic design is considered when the two ternary elements intersect themselves. The optimal kinematic design in terms of size and height variation will result from the optimized synthesis method. That being said, the difference between these structures is given by a design coefficient p (where p < 1 for Figure 1 and p > 1 for Figure 2) that states the relationship between the links l_{31} and l_{3} as follows:

$$l_{31} = p \cdot l_3 \tag{5}$$

which results in the following:

$$l_3 = l_{31} + l_{32} \tag{6}$$

for the structure presented in Figure 1, and the following:

$$l_{31} = l_3 + l_{32} (7)$$

for the structure presented in Figure 2.

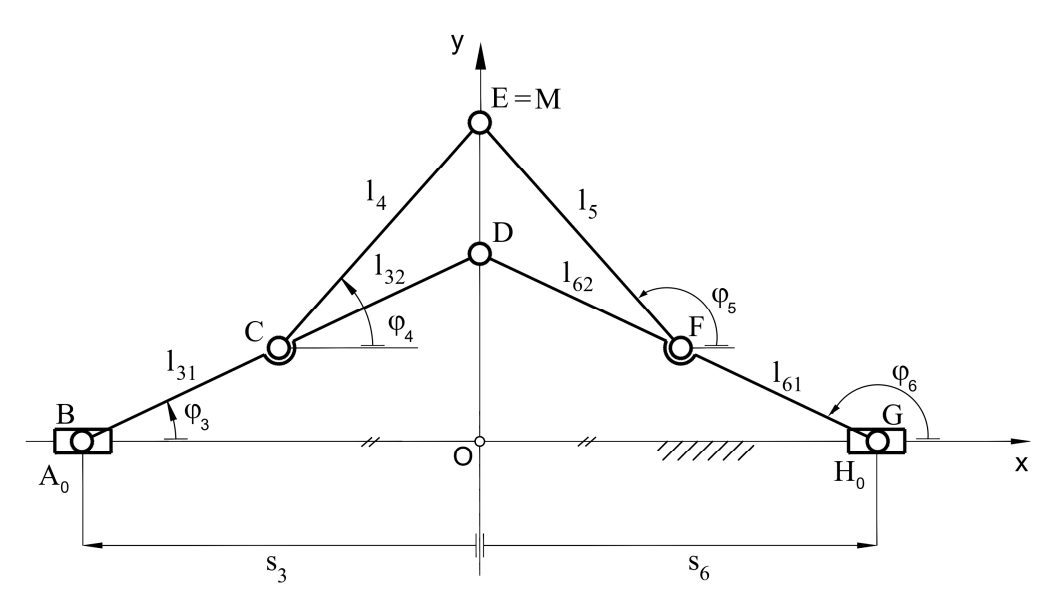


Figure 1. Kinematic scheme of the seven-bar linkage 7- $\underline{P}R(RRRR)R\underline{P}$ when p < 1 [15].

These structures are feasible for the design of a medical disinfection robot because they provide a high variation of both the stroke and height from the folded position to the extended position, thus being able to perform in different configurations and disinfect different types of environments in medical facilities.

Due to design and functional requirements, the length of the strokes s_3 and s_6 (henceforth referred to only as s) and the length of the elements l_4 and l_5 were chosen to be equal, respectively, as well as the length of the links l_{31} , l_{32} , l_{61} , and l_{62} (for the structure presented in Figure 1) and the length of the links l_3 , l_{32} , l_6 , and l_{62} (for the structure presented in Figure 2).

Robotics **2024**, 13, 177 5 of 24

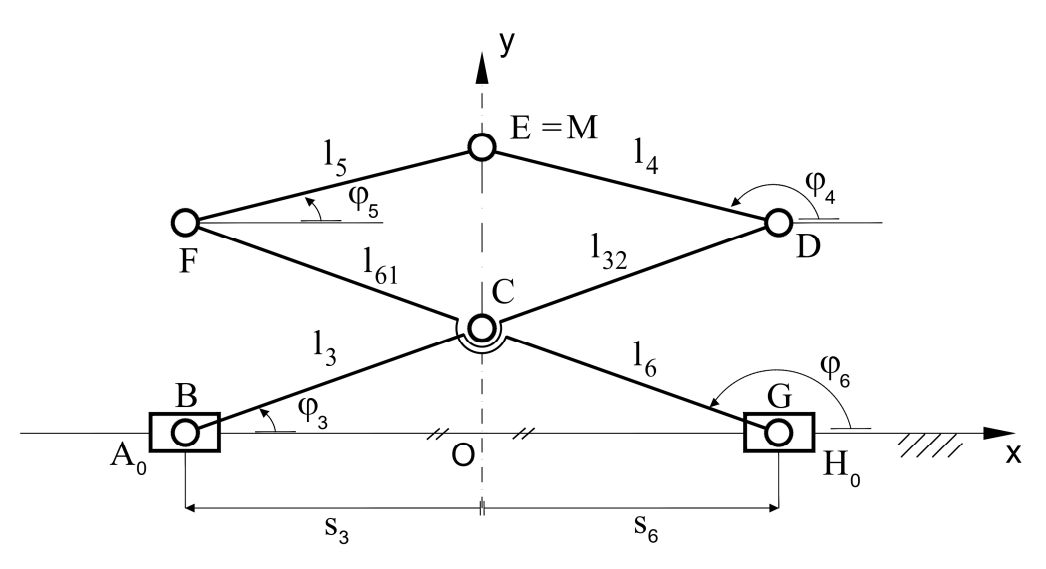


Figure 2. Kinematic scheme of the seven-bar linkage 7- $\underline{P}R(RRR)R\underline{P}$ when p > 1.

The aim of the analytical synthesis of the seven-bar linkage is to compute the lengths of the elements in order to avoid singularities in the trajectory of characteristic point M. Therefore, it is necessary to avoid the collinearity between the mobile neighboring links in the folded and extended configuration of the mechanism.

The first condition states that the length of the element l_4 needs to be greater than the length of the link l_{32} in order to avoid the collinearity between them:

$$l_4 > l_{32}$$
 (8)

which results in the following:

$$l_4 > l_3 - l_{31} \tag{9}$$

when p < 1, and the following:

$$l_4 > l_{31} - l_3 \tag{10}$$

when p > 1.

The second condition is necessary in order to avoid the collinearity between the stroke and the element l_3 , so that the folded configuration of the mechanism is avoided:

$$l_3 > s_{max} \tag{11}$$

In order to obtain the analytical solution of the synthesis, the inequalities system given by Equations (9)–(11) can be substituted with an equations system by imposing a coefficient k > 1. The lower end of each inequation is multiplied with k in order to avoid the collinearity between the mobile neighboring links of the mechanism. The resulting equations system can be expressed as follows:

$$l_4 = k \cdot (l_3 - l_{31}) \tag{12}$$

when p < 1, and as follows:

$$l_4 = k \cdot (l_{31} - l_3) \tag{13}$$

when p > 1.

$$l_3 = k \cdot s_{max} \tag{14}$$

Furthermore, by applying the fundamental theorem of similarity and by using Equations (12)–(14), the stroke s, as s_{max} , for the folded position of the linkage, can be computed as follows:

$$s_{max} = \frac{y_{min}}{\sqrt{k^2 - 1 \cdot \left[p + (1 - p) \cdot \sqrt{k^2 + 1} \right]}}$$
 (15)

Robotics **2024**, 13, 177 6 of 24

when p < 1, and as follows:

$$s_{max} = \frac{y_{min}}{\sqrt{k^2 - 1} \cdot \left[p + (p - 1) \cdot \sqrt{k^2 + 1} \right]}$$
 (16)

when p > 1.

For the extended position of the linkage, the stroke s (as s_{min}) and the y coordinate of the characteristic point M (as y_{max}) can be computed by imposing the maximum value of the angle φ_3 , as follows:

$$s_{min} = l_3 \cdot \cos(\varphi_{3_{max}}) \tag{17}$$

$$y_{max} = l_3 \cdot \sin(\varphi_{3_{max}}) + l_4 \cdot \sin\left(\arccos\left(\frac{l_{32} \cdot s_{min}}{l_4 \cdot (l_{31} + l_{32})}\right)\right)$$
 (18)

when p < 1, and as follows:

$$y_{max} = l_3 \cdot \sin(\varphi_{3_{max}}) + l_{32} \cdot \sin(\varphi_{3_{max}}) + l_4 \cdot \sin(\varphi_{3_{max}})$$

$$\tag{19}$$

when p > 1.

3. Results of the Synthesis

Table 3 shows the results of the synthesis method by considering as input parameters the minimum height of the seven-bar linkage (also referred as the y coordinate of the characteristic point M) $y_{min} = 150$ mm, the coefficient k = 1.3, the maximum value of the positional angle $\varphi_{3max} = 60^{\circ}$, and the design coefficient p in the range of (0; 2].

Parameter	p = 0.25	p = 0.5	p = 0.75	p = 1.25	p = 1.5	p = 1.75	<i>p</i> = 2	Unit
l ₃₁	39.65	88.91	151.77	176.76	151.77	137.85	128.98	[mm]
l ₃₂	118.95	88.91	50.59	35.35	50.59	59.08	64.49	[mm]
l_3	158.60	177.83	202.36	141.41	101.18	78.77	64.49	[mm]
l_4	154.64	115.59	65.76	45.95	65.76	76.80	83.83	[mm]
s_{min}	67.03	75.15	85.52	59.76	42.76	33.29	27.25	[mm]
S _{max}	122.00	136.79	155.66	108.78	77.83	60.59	49.60	[mm]
$arphi_{3_{min}}$	39.71	39.71	39.71	39.71	39.71	39.71	39.71	[°]
y _{max}	184.50	191.63	200.74	201.86	197.16	194.54	192.87	[mm]

Table 3. Resulted parameters of the seven-bar linkage for k = 1.3 and different values of p.

The value of the coefficient k was arbitrary given just to exemplify the initial results of the synthesis method and to show the possible resulted structures. It will also highlight the necessity for an optimized synthesis method, since arbitrarily choosing the coefficient k or the design coefficient p does not guarantee that we will obtain the optimal seven-bar linkage structure.

The next three figures show the resulting seven-bar linkages 7-PR(RRRR)RP in the folded position (minimum configuration) and in the extended position (maximum configuration) computed with the parameters presented in Table 3 for different values of the design coefficient p < 1.

Figure 3 presents the resulting seven-bar linkage 7- $\underline{P}R(RRRR)R\underline{P}$ computed with the coefficient k = 1.3 and the design coefficient p = 0.25. The maximum total height of the mechanism computed with these parameters is $y_{max} = 184.5$ mm, while the total size is 244 mm.

Robotics **2024**, 13, 177 7 of 24

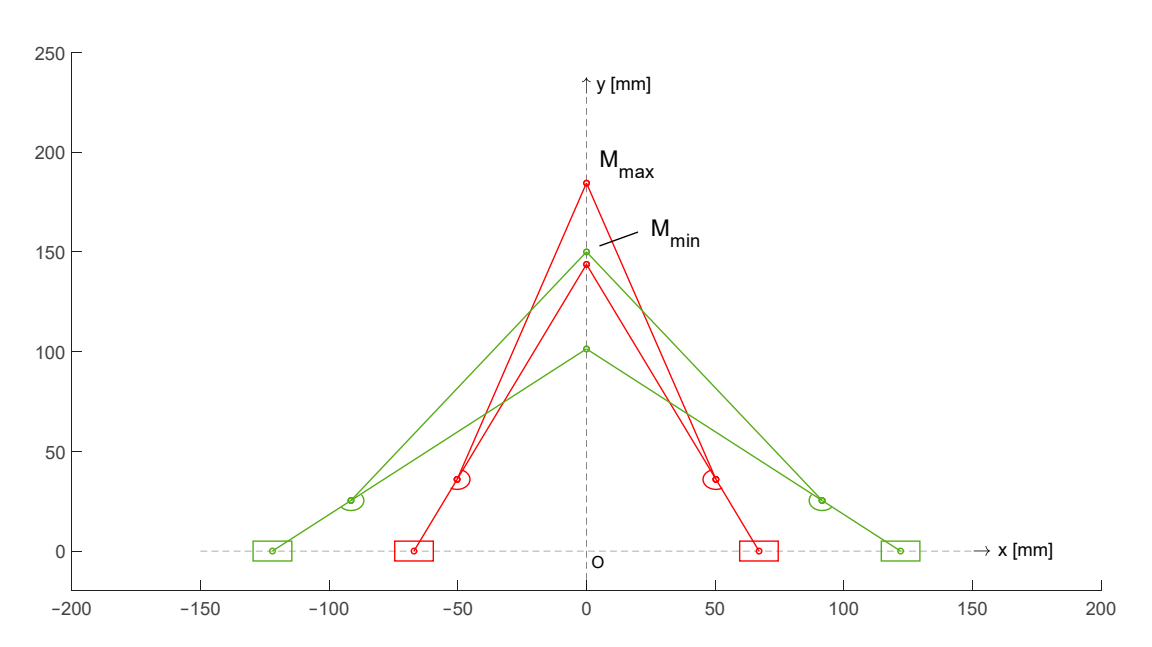


Figure 3. The seven-bar linkage computed with k = 1.3 and p = 0.25 in its folded position (green) and extended position (red).

Figure 4 presents the resulting seven-bar linkage 7- $\underline{P}R(RRR)R\underline{P}$ computed with the coefficient k=1.3 and the design coefficient p=0.5. The maximum total height of the mechanism computed with these parameters is $y_{max}=191.63$ mm, while the total size is 273.58 mm. It can be observed that both the total height and the total size of the seven-bar linkage increase directly proportional to the design coefficient p.

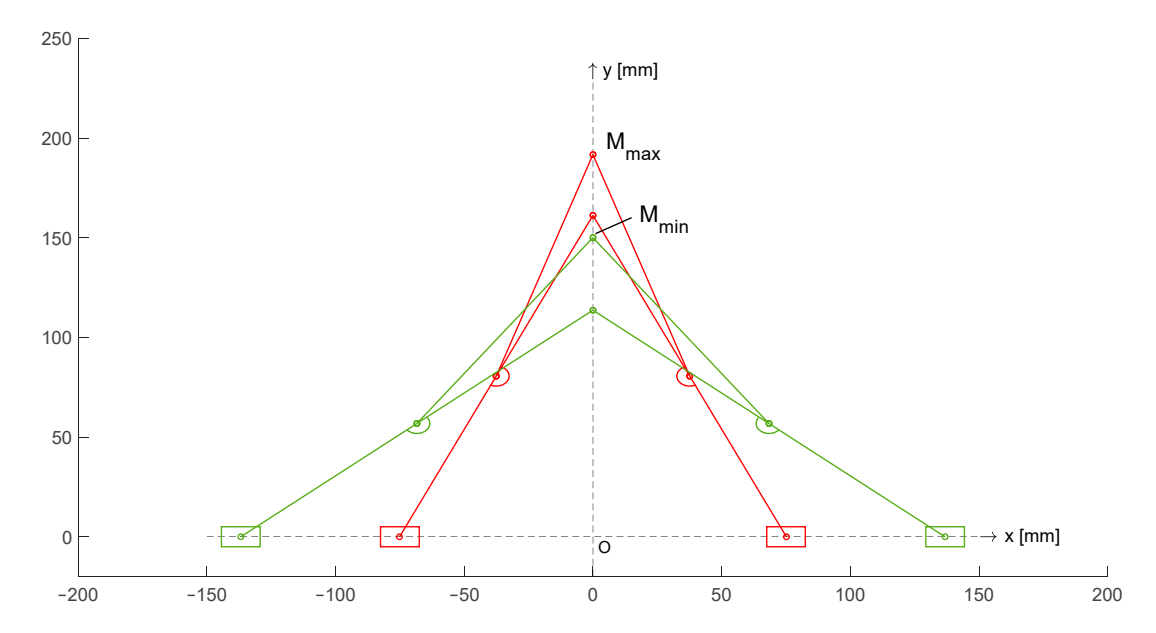


Figure 4. The seven-bar linkage computed with k = 1.3 and p = 0.5 in its folded position (green) and extended position (red).

Figure 5 presents the resulting seven-bar linkage 7- $\underline{P}R(RRR)R\underline{P}$ computed with coefficients k=1.3 and p=0.75. The maximum height of the mechanism with these parameters is $y_{max}=200.74$ mm, while the total size is 311.32 mm.

As a conclusion, for a design coefficient p < 1, it can be noted that both the total size and the total height of the mechanism increase directly proportional to the design coefficient p. Moreover, the length of the links l_{31} and l_{3} increase directly proportional to the design

Robotics **2024**, 13, 177 8 of 24

coefficient p, while the length of the links l_{32} and l_4 decrease directly proportional to the design coefficient p.

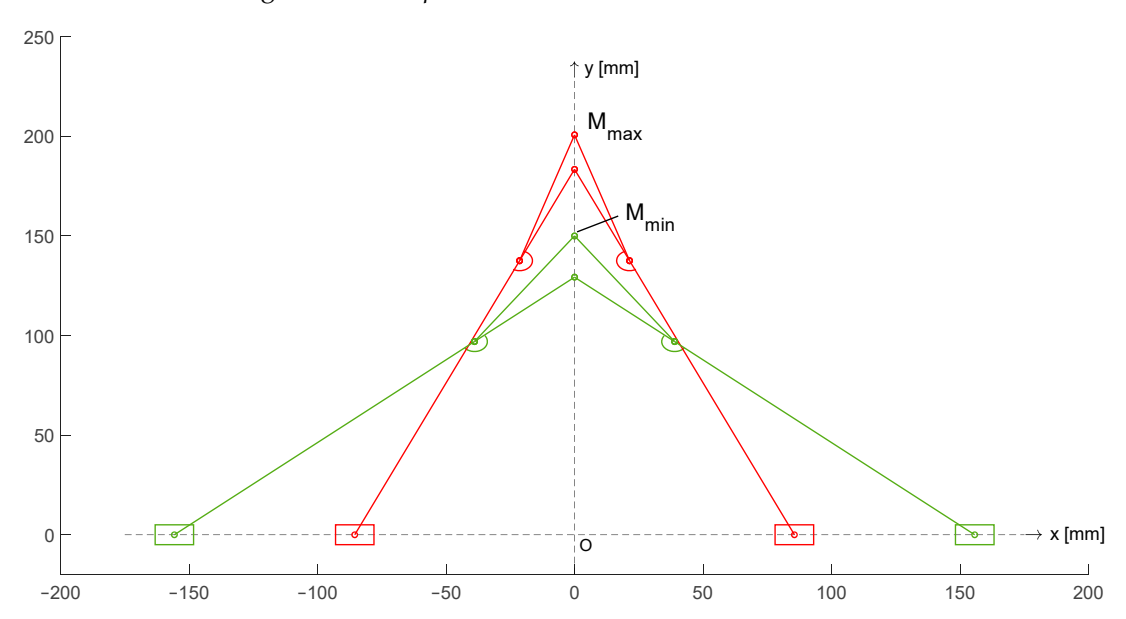


Figure 5. The seven-bar linkage computed with k = 1.3 and p = 0.75 in its folded position (green) and extended position (red).

The next four figures show the resulting seven-bar linkages $7-\underline{P}R(RRRR)R\underline{P}$ in the folded position (minimum configuration) and in the extended position (maximum configuration), computed with the parameters presented in Table 1 for a design coefficient p > 1.

Figure 6 presents the resulting seven-bar linkage 7-PR(RRRR)RP computed with coefficients k = 1.3 and p = 1.25. The maximum height of the mechanism with these parameters is $y_{max} = 201.86$ mm, while the total size is 217.56 mm. It can be observed that the total height of the mechanism is higher than the one computed with p = 0.75, but the total size of the mechanism is considerably smaller than the one computed with p = 0.75, which had a value of 311.32 mm.

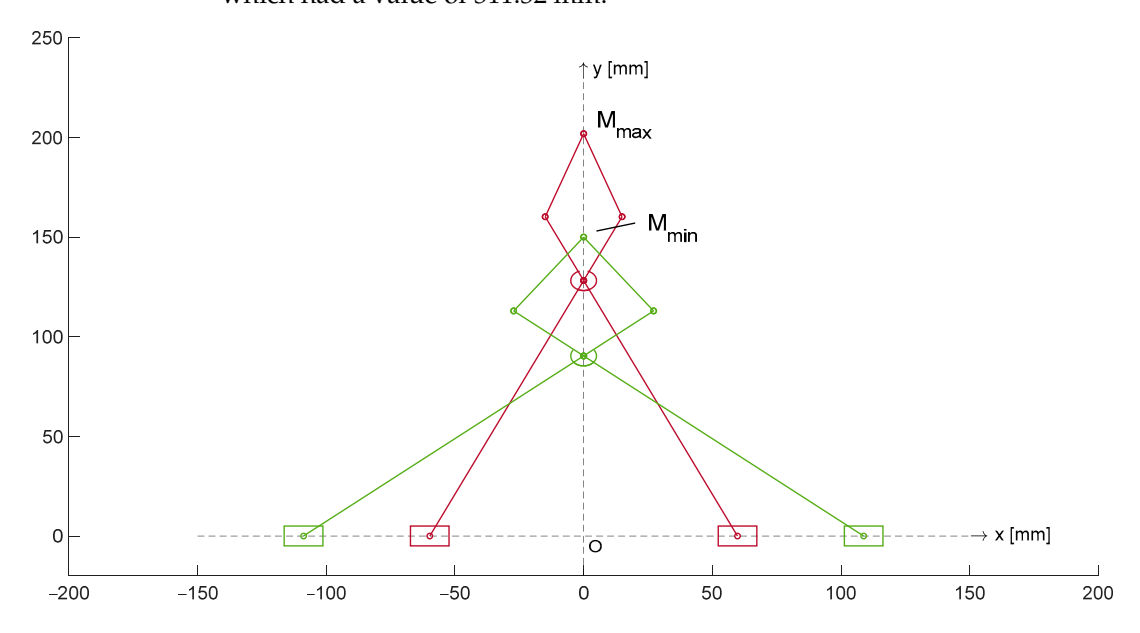


Figure 6. The seven-bar linkage computed with k = 1.3 and p = 1.25 in its folded position (green) and extended position (red).

Robotics **2024**, 13, 177 9 of 24

Figure 7 presents the resulting seven-bar linkage 7- $\underline{P}R(RRR)R\underline{P}$ computed with coefficients k = 1.3 and p = 1.5. The maximum height of the mechanism with these parameters is $y_{max} = 197.16$ mm, while the total size is 155.66 mm. It can be observed that the total height of the mechanism tends to decrease slightly, but not so much as the total size.

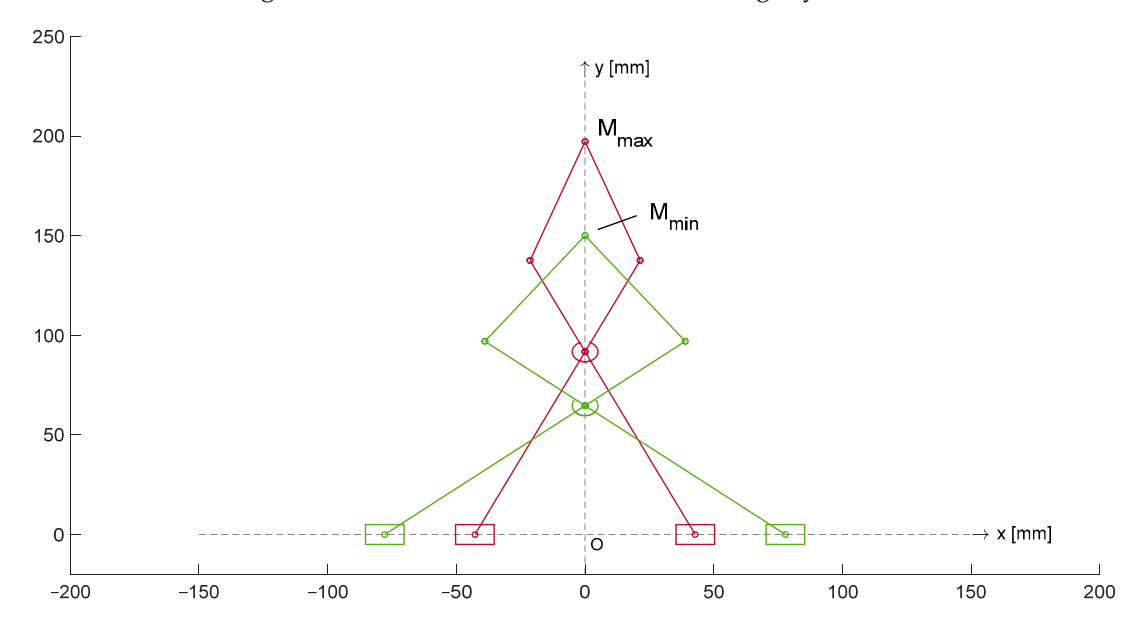


Figure 7. The seven-bar linkage computed with k = 1.3 and p = 1.5 in its folded position (green) and extended position (red).

Figure 8 presents the resulting seven-bar linkage 7- $\underline{P}R(RRR)R\underline{P}$ computed with coefficients k=1.3 and p=1.75. The maximum height of the mechanism with these parameters is $y_{max}=194.54$ mm, while the total size is 121.18 mm.

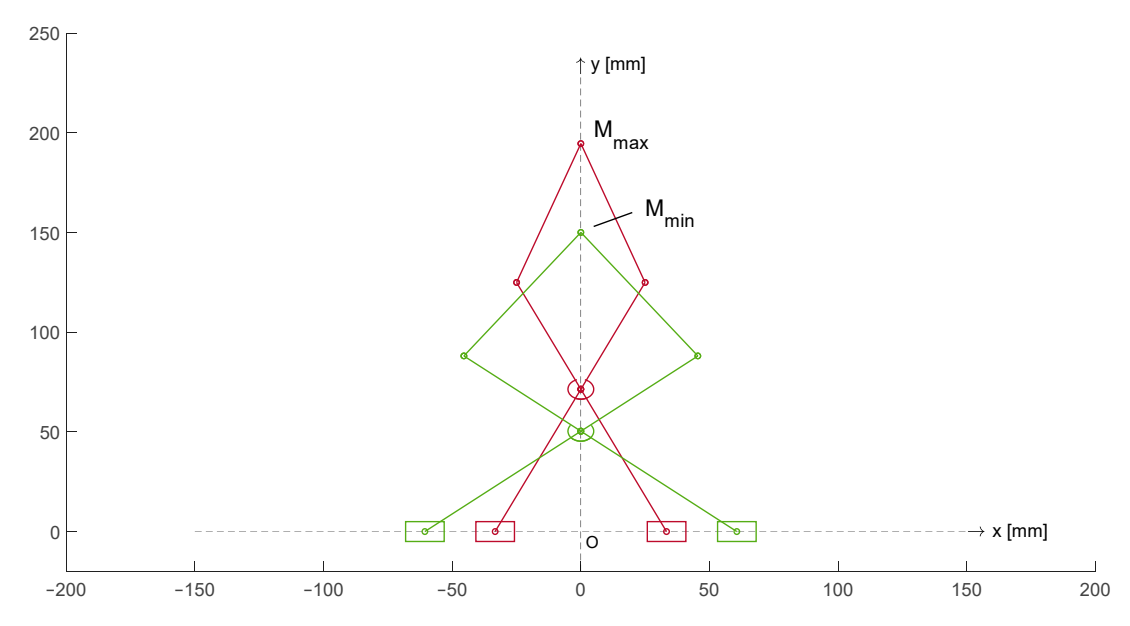


Figure 8. The seven-bar linkage computed with k = 1.3 and p = 1.75 in its folded position (green) and extended position (red).

Figure 9 presents the presents the resulting seven-bar linkage 7- $\underline{P}R(RRRR)R\underline{P}$ computed with coefficients k = 1.3 and p = 2. The maximum height of the mechanism with these parameters is $y_{max} = 192.87$ mm, while the total size is 99.2 mm.

Robotics **2024**, 13, 177 10 of 24

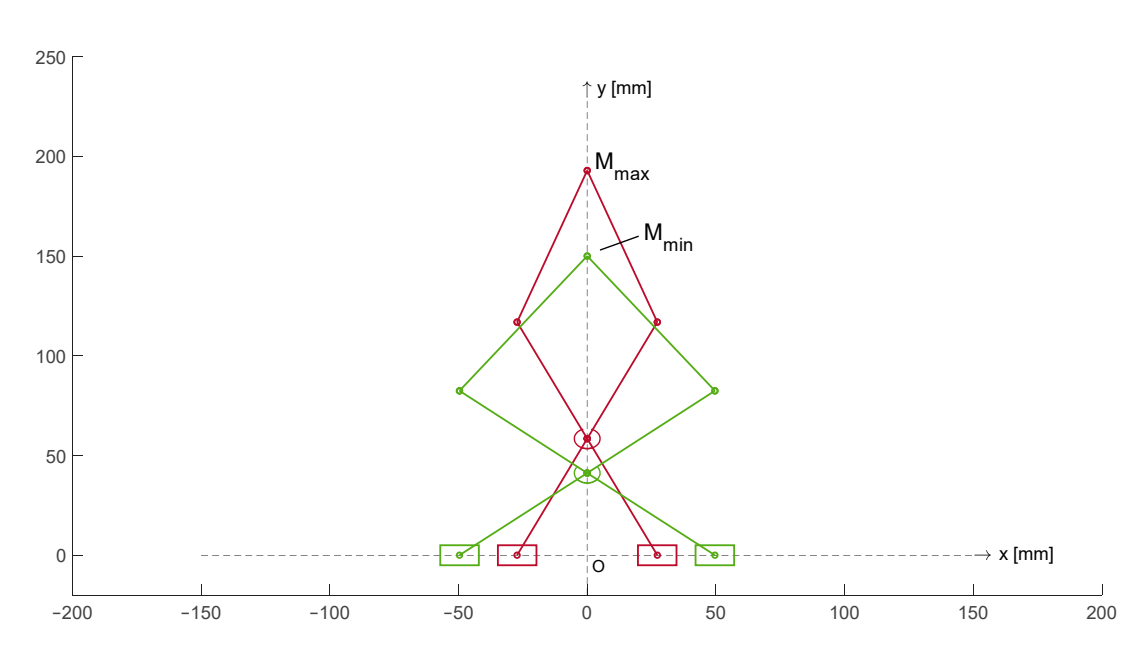


Figure 9. The seven-bar linkage computed with k = 1.3 and p = 2 in its folded position (green) and extended position (red).

As a conclusion, for the seven-bar linkages computed with a design coefficient p > 1, it must be noted that the total size of the mechanism decreased significantly compared to the total size computed with a design coefficient p < 1, while the values of the total height of the mechanism did not change very much.

4. Optimized Synthesis Method of the Symmetrical Seven-Bar Linkage

The optimized synthesis method takes into consideration the height and the size of the 7-PR(RRRR)RP seven-bar linkage. In particular, the aim is to achieve the best ratio between the height range of the mechanism, which needs to be as high as possible, and the total size of the mechanism, which needs to be as low as possible. Subsequently, the variable of all parameters, the length of the links $l_3(k)$, $l_{31}(k)$, $l_{32}(k)$, and $l_4(k)$ and the minimum input transmission angle $\mu_{3_{min}}(k)$ (which is equal to $\varphi_{3_{min}}$) will be the coefficient k > 1. The height of the mechanism in the folded position (the y coordinate of the characteristic point M, y_{min}) as well as the maximum value of the positional angle φ_3 are considered input data and therefore their values are known.

The maximum value for the height of the mechanism, also referred as the y coordinate of the characteristic point M in the extended position, y_{max} , can be computed using Equations (18) and (19):

$$y_{max}(k) = l_3(k) \cdot \sin(\varphi_{3_{max}}) + l_4(k) \cdot \sin\left(\arccos\left(\frac{l_{32}(k) \cdot s_{min}(k)}{l_4(k) \cdot (l_{31}(k) + l_{32}(k))}\right)\right)$$
(20)

when p < 1, and as follows:

$$y_{max}(k) = l_3(k) \cdot \sin(\varphi_{3_{max}}) + l_{32}(k) \cdot \sin(\varphi_{3_{max}}) + l_4(k) \cdot \sin(\varphi_{3_{max}})$$
(21)

when p > 1.

The minimum possible value for the total size of the mechanism is considered as the double value of its stroke in the folded position, s_{max} , which can be computed using Equations (15) and (16):

$$s_{max}(k) = \frac{y_{min}}{\sqrt{k^2 - 1} \cdot \left[p + (1 - p) \cdot \sqrt{k^2 + 1} \right]}$$
 (22)

Robotics 2024, 13, 177 11 of 24

$$L_x = 2 \cdot s_{max}(k) = \frac{2 \cdot y_{min}}{\sqrt{k^2 - 1} \cdot \left[p + (1 - p) \cdot \sqrt{k^2 + 1} \right]}$$
 (23)

when p < 1, and as follows:

$$s_{max}(k) = \frac{y_{min}}{\sqrt{k^2 - 1 \cdot \left[p + (p - 1) \cdot \sqrt{k^2 + 1} \right]}}$$
 (24)

$$L_x = 2 \cdot s_{max}(k) = \frac{2 \cdot y_{min}}{\sqrt{k^2 - 1} \cdot \left[p + (p - 1) \cdot \sqrt{k^2 + 1} \right]}$$
 (25)

when p > 1.

The length of the links, the minimum input transmission angle $\mu_{3_{min}}$ and the stroke of the mechanism in the extended position are expressed using Equations (5)–(7), (12)–(14) and (17):

$$l_3(k) = k \cdot s_{max}(k) \tag{26}$$

$$l_{31}(k) = p \cdot l_3(k) \tag{27}$$

$$l_{32}(k) = l_3(k) - l_{31}(k) (28)$$

when p < 1, and as follows:

$$l_{32}(k) = l_{31}(k) - l_3(k) (29)$$

when p > 1.

$$l_4(k) = k \cdot l_{32}(k) \tag{30}$$

$$\mu_{3_{min}}(k) = \arccos \frac{s_{\max}(k)}{l_3(k)} \tag{31}$$

$$s_{\min}(k) = l_3(k) \cdot \cos(\varphi_{3_{\max}}) \tag{32}$$

The target function for the optimization problem is computed using the normalized values of the maximum height of the mechanism, $\overline{y_{max}}(k)$, and the normalized values of the total size of the mechanism, $\overline{L_x}(k)$, each of them having an imposed weight coefficient, c_1 and c_2 . The target function should be maximized in order to obtain the optimal value for the coefficient k:

$$F(k) = c_1 \cdot \overline{y_{max}}(k) - c_2 \cdot \overline{L_x}(k) \to \max$$
 (33)

where:

$$\overline{y_{max}}(k) = \frac{y_{max}(k) - y_{max}(k)|_{min}}{y_{max}(k)|_{max} - y_{max}(k)|_{min}}$$
(34)

and:

$$\overline{L_x}(k) = \frac{L_x(k) - L_x(k)|_{min}}{L_x(k)|_{max} - L_x(k)|_{min}}$$
(35)

5. Results of the Optimized Synthesis Method

The input parameters, as the minimum height of the mechanism y_{min} and the maximum value of the positional angle φ_3 , are given in Table 4. The coefficient k is defined in the range of [1.1; 2], the design coefficient p is defined in the range of (0; 2], and the weight coefficients c_1 and c_2 are considered to be 0.5.

Table 4. Input parameters of the seven-bar linkage.

Parameter	Value
${\cal Y}_{min} \ arphi_{3_{max}}$	150 mm 60°

Robotics 2024, 13, 177 12 of 24

The following tables highlight the results of the optimized synthesis method by showing the variation of the mechanism's output parameters for coefficient $k \in [1.1; 2]$ and design coefficient $p \in [0.25; 2]$.

Table 5 presents the computed values of the lengths of the link l_3 . As can be observed, the length of the link l_3 decreases while coefficients k and p increase. The maximum value of the link l_3 is obtained for k = 1.1 and p = 0.75, while its minimum value is obtained for k = 2 and p = 2.

l_3 [mm]										
k	p = 0.25	p = 0.5	p = 0.75	p = 1.25	<i>p</i> = 1.5	<i>p</i> = 1.75	p = 2			
<i>k</i> = 1.1	263.78	289.59	321.00	222.03	160.50	125.67	103.26			
k = 1.2	190.89	211.83	237.92	165.41	118.96	92.88	76.18			
k = 1.3	158.60	177.83	202.36	141.41	101.18	78.77	64.49			
k = 1.4	139.14	157.56	181.61	127.56	90.80	70.49	57.60			
k = 1.5	125.61	143.60	167.60	118.33	83.80	64.87	52.92			
k = 1.6	115.40	133.12	157.28	111.60	78.64	60.71	49.43			
k = 1.7	107.26	124.80	149.21	106.41	74.60	57.43	46.69			
k = 1.8	100.53	117.94	142.63	102.22	71.31	54.76	44.44			
k = 1.9	94.82	112.11	137.09	98.73	68.54	52.49	42.53			
k = 2	89.88	107.04	132.31	95.74	66.15	50.54	40.88			

Table 6 presents the computed values of the lengths of the link l_{31} . As can be seen, the maximum value of the link l_{31} is obtained for k = 1.1 and p = 1.25, while its minimum value is obtained for k = 2 and p = 0.25.

Table 6. Results of the lengths of the link l_{31} .

l_{31} [mm]										
k	p = 0.25	p = 0.5	p = 0.75	p = 1.25	<i>p</i> = 1.5	p = 1.75	p = 2			
k = 1.1	65.94	144.79	240.75	277.54	240.75	219.93	206.53			
k = 1.2	47.72	105.91	178.44	206.76	178.44	162.54	152.36			
k = 1.3	39.65	88.91	151.77	176.76	151.77	137.85	128.98			
k = 1.4	34.78	78.78	136.21	159.46	136.21	123.36	115.21			
k = 1.5	31.40	71.80	125.70	147.91	125.70	113.53	105.84			
k = 1.6	28.85	66.56	117.96	139.50	117.96	106.24	98.87			
k = 1.7	26.81	62.40	111.91	133.01	111.91	100.51	93.38			
k = 1.8	25.13	58.97	106.97	127.77	106.97	95.83	88.88			
k = 1.9	23.70	56.05	102.82	123.41	102.82	91.87	85.07			
k = 2	22.47	53.52	99.23	119.68	99.23	88.44	81.77			

Table 7 presents the computed values of the lengths of the link l_{32} . As can be observed, the length of the link l_{32} considerably smaller than the length of the links l_3 and l_{31} . Its maximum value is computed for k = 1.1 and p = 0.25, while its minimum value is obtained for k = 2 and p = 1.25.

Table 8 presents the computed values of the lengths of the link l_4 . It can be seen that its values are considerably larger when $p \in [0.25; 0.5]$, the maximum value being obtained

Robotics 2024, 13, 177 13 of 24

for coefficients k = 1.1 and p = 0.25. Smaller values of the length of the link l_4 are computed for design coefficient $p \in [0.75; 1.75]$, the lowest value being obtained for the coefficients k = 1.5 and p = 1.25.

Table 7	. Results	of the	lengths	of the	link l_{32} .
---------	-----------	--------	---------	--------	-----------------

			l ₃₂ [:	mm]			
k	p = 0.25	p = 0.5	p = 0.75	p = 1.25	<i>p</i> = 1.5	p = 1.75	<i>p</i> = 2
k = 1.1	197.84	144.79	80.25	55.50	80.25	94.25	103.26
k = 1.2	143.16	105.91	59.48	41.35	59.48	69.66	76.18
k = 1.3	118.95	88.91	50.59	35.35	50.59	59.08	64.49
k = 1.4	104.35	78.78	45.40	31.89	45.40	52.87	57.60
k = 1.5	94.21	71.80	41.90	29.58	41.90	48.65	52.92
k = 1.6	86.55	66.56	39.32	27.90	39.32	45.53	49.43
k = 1.7	80.44	62.40	37.30	26.60	37.30	43.07	46.69
k = 1.8	75.40	58.97	35.65	25.55	35.65	41.07	44.44
k = 1.9	71.12	56.05	34.27	24.68	34.27	39.37	42.53
k = 2	67.41	53.52	33.07	23.93	33.07	37.90	40.88

Table 8. Results of the lengths of the link l_4 .

	$l_4[mm]$										
k	p = 0.25	p = 0.5	p = 0.75	p = 1.25	p = 1.5	p = 1.75	<i>p</i> = 2				
k = 1.1	217.62	159.27	88.27	61.05	88.27	103.68	113.59				
<i>k</i> = 1.2	171.80	127.09	71.37	49.62	71.37	83.59	91.41				
k = 1.3	154.64	115.59	65.76	45.95	65.76	76.80	83.83				
k = 1.4	146.10	110.29	63.56	44.64	63.56	74.02	80.65				
k = 1.5	141.31	107.70	62.85	44.37	62.85	72.98	79.38				
k = 1.6	138.48	106.50	62.91	44.64	62.91	72.85	79.10				
k = 1.7	136.76	106.08	63.41	45.22	63.41	73.23	79.38				
k = 1.8	135.72	106.14	64.18	46.00	64.18	73.92	79.99				
k = 1.9	135.13	106.50	65.12	46.89	65.12	74.80	80.82				
<i>k</i> = 2	134.82	107.04	66.15	47.87	66.15	75.81	81.77				

Table 9 presents the computed values of the minimum input transmission angle $\mu_{3_{min}}$. As can be observed, the values of $\mu_{3_{min}}$ do not depend on the value of the design coefficient p. The lowest value of the minimum input transmission angle is obtained for coefficient k = 1.1, while its highest value is obtained for k = 2.

Table 10 presents the computed values of the mechanism's stroke in the extended position s_{min} . The maximum stroke value in the extended position of the seven-bar linkage 7-PR(RRRR)RP is achieved for the coefficients k = 1.1 and p = 0.75, while the minimum stroke value in the same configuration of the mechanism is computed with coefficients k = 2 and p = 2.

Table 11 presents the computed values of the mechanism's stroke in the folded position s_{max} . The maximum stroke value in the folded position of the seven-bar linkage 7-PR(RRRR)RP is achieved once again, just like in the previous case, for the coefficients k = 1.1 and p = 0.75, while the minimum stroke value of the mechanism is computed with coefficients k = 2 and p = 2.

Robotics 2024, 13, 177 14 of 24

Table 9. Results of the minimum input transmission angle $\mu_{3_{min}}$.

	$\mu_{3_{min}}$ [°]										
k	p = 0.25	p = 0.5	p = 0.75	p = 1.25	<i>p</i> = 1.5	p = 1.75	p = 2				
k = 1.1	24.61	24.61	24.61	24.61	24.61	24.61	24.61				
k = 1.2	33.55	33.55	33.55	33.55	33.55	33.55	33.55				
k = 1.3	39.71	39.71	39.71	39.71	39.71	39.71	39.71				
k = 1.4	44.41	44.41	44.41	44.41	44.41	44.41	44.41				
k = 1.5	48.18	48.18	48.18	48.18	48.18	48.18	48.18				
k = 1.6	51.31	51.31	51.31	51.31	51.31	51.31	51.31				
k = 1.7	53.96	53.96	53.96	53.96	53.96	53.96	53.96				
k = 1.8	56.25	56.25	56.25	56.25	56.25	56.25	56.25				
k = 1.9	58.24	58.24	58.24	58.24	58.24	58.24	58.24				
<i>k</i> = 2	60.00	60.00	60.00	60.00	60.00	60.00	60.00				

Table 10. Results of the lengths of the stroke s in the extended position (s_{min}).

s_{min} [mm]										
k	p = 0.25	p = 0.5	p = 0.75	p = 1.25	p = 1.5	p = 1.75	p = 2			
k = 1.1	111.48	122.38	135.66	93.83	67.83	53.11	43.64			
k = 1.2	80.67	89.52	100.55	69.90	50.27	39.25	32.19			
k = 1.3	67.03	75.15	85.52	59.76	42.76	33.29	27.25			
k = 1.4	58.80	66.59	76.75	53.91	38.37	29.79	24.34			
k = 1.5	53.08	60.69	70.83	50.00	35.41	27.41	22.36			
k = 1.6	48.77	56.26	66.47	47.16	33.23	25.65	20.89			
k = 1.7	45.33	52.74	63.06	44.97	31.53	24.27	19.73			
k = 1.8	42.48	49.84	60.27	43.20	30.13	23.14	18.78			
k = 1.9	40.07	47.37	57.93	41.72	28.96	22.18	17.97			
k = 2	37.98	45.23	55.91	40.46	27.95	21.35	17.28			

Table 11. Results of the lengths of the stroke s in the folded position (s_{max}).

s_{max} [mm]							
k	p = 0.25	p = 0.5	p = 0.75	p = 1.25	p = 1.5	p = 1.75	<i>p</i> = 2
k = 1.1	239.80	263.27	291.82	201.84	145.91	114.25	93.88
k = 1.2	159.07	176.52	198.27	137.84	99.13	77.40	63.48
k = 1.3	122.00	136.79	155.66	108.78	77.83	60.59	49.60
k = 1.4	99.38	112.54	129.72	91.12	64.86	50.35	41.14
k = 1.5	83.74	95.73	111.73	78.88	55.86	43.24	35.28
k = 1.6	72.12	83.20	98.30	69.75	49.15	37.94	30.89
k = 1.7	63.09	73.41	87.77	62.59	43.88	33.78	27.46
k = 1.8	55.85	65.52	79.24	56.79	39.62	30.42	24.69
k = 1.9	49.90	59.00	72.15	51.96	36.07	27.63	22.38
k = 2	44.94	53.52	66.15	47.87	33.07	25.27	20.44

Robotics 2024, 13, 177 15 of 24

Table 12 presents the computed values of the maximum height of the seven-bar linkage 7-PR(RRRR)RP, y_{max} , achieved in the extended position of the mechanism. As can be observed, the highest value of y_{max} is computed for coefficients k = 1.1 and p = 1.25, while the lowest value is computed for coefficients k = 2 and k = 2.

Table 13 presents the computed values of the total size of the seven-bar linkage 7- $\underline{P}R(RRR)R\underline{P}$, L_x . It can be observed that the values of L_x decrease while the values of the coefficients k and p increase. The largest total size of the mechanism L_x is obtained for coefficients k = 1.1 and p = 0.75, while the lowest total size is obtained for coefficients k = 2 and k = 2.

	y_{max} [mm]						
k	p = 0.25	p = 0.5	p = 0.75	p = 1.25	p = 1.5	p = 1.75	p = 2
k = 1.1	260.69	278.28	299.70	306.87	298.20	293.29	290.14
k = 1.2	204.04	214.94	228.53	232.36	226.41	223.07	220.93
k = 1.3	182.17	189.90	199.75	201.86	197.16	194.54	192.87
k = 1.4	170.81	176.55	184.05	184.98	181.06	178.89	177.51
k = 1.5	164.05	168.41	174.23	174.27	170.89	169.03	167.86
k = 1.6	159.71	163.04	167.59	166.89	163.92	162.31	161.30
k = 1.7	156.77	159.31	162.85	161.54	158.90	157.47	156.58
k = 1.8	154.71	156.62	159.34	157.49	155.12	153.85	153.06
k = 1.9	153.23	154.63	156.67	154.35	152.20	151.06	150.35
k = 2	152.14	153.13	154.60	151.85	149.89	148.86	148.22

Table 13. Results of the total size of the mechanism L_x .

L_x [mm]							
k	p = 0.25	p = 0.5	p = 0.75	p = 1.25	p = 1.5	p = 1.75	<i>p</i> = 2
k = 1.1	479.61	526.54	583.65	403.69	291.82	228.50	187.76
k = 1.2	318.15	353.05	396.54	275.68	198.27	154.80	126.96
k = 1.3	244.01	273.59	311.33	217.56	155.66	121.19	99.21
k = 1.4	198.77	225.09	259.45	182.24	129.72	100.70	82.29
k = 1.5	167.48	191.47	223.47	157.77	111.73	86.49	70.56
k = 1.6	144.25	166.40	196.60	139.50	98.30	75.88	61.79
k = 1.7	126.19	146.83	175.54	125.19	87.77	67.57	54.93
k = 1.8	111.70	131.04	158.48	113.58	79.24	60.84	49.38
k = 1.9	99.81	118.01	144.31	103.92	72.15	55.26	44.77
<i>k</i> = 2	89.88	107.04	132.31	95.74	66.15	50.54	40.88

Table 14 shows the computed values of the target function F(k) of the seven-bar linkage 7-PR(RRR), which considered the normalized values of the total height and total size of the mechanism.

As already mentioned before, the target function should be maximized in order to obtain the optimal value for the coefficient k. The maximum value of the target function F(k) is obtained for the coefficients k = 1.1 and p = 2, which indicates the optimized seven-bar linkage.

The corresponding lengths of the links l_{31} , l_{32} , l_{3} , and l_{4} , the minimum stroke s_{min} , the maximum stroke s_{max} , the minimum input transmission angle $\mu_{3_{min}}$, the total height of the mechanism y_{max} and the total size of the mechanism L_x are further presented in Table 15.

Robotics **2024**, 13, 177 16 of 24

Table 14. Target function of	output for different values	of the variables k and n .

			F((k)			
k	p = 0.25	p = 0.5	p = 0.75	p = 1.25	p = 1.5	p = 1.75	p = 2
k = 1.1	-0.0497	-0.0375	-0.0226	0.1658	0.2415	0.2844	0.3120
k = 1.2	-0.0795	-0.0773	-0.0745	0.0489	0.1014	0.1310	0.1499
k = 1.3	-0.0801	-0.0830	-0.0868	0.0063	0.0485	0.0720	0.0870
k = 1.4	-0.0743	-0.0804	-0.0884	-0.0144	0.0216	0.0415	0.0542
k = 1.5	-0.0667	-0.0751	-0.0862	-0.0256	0.0062	0.0236	0.0346
k = 1.6	-0.0590	-0.0689	-0.0824	-0.0320	-0.0034	0.0122	0.0219
k = 1.7	-0.0517	-0.0627	-0.0780	-0.0357	-0.0096	0.0046	0.0134
k = 1.8	-0.0448	-0.0566	-0.0733	-0.0378	-0.0136	-0.0006	0.0074
k = 1.9	-0.0385	-0.0508	-0.0686	-0.0388	-0.0163	-0.0043	0.0031
<i>k</i> = 2	-0.0328	-0.0455	-0.0641	-0.0391	-0.0180	-0.0069	0

Table 15. Geometrical parameters of the optimized seven-bar linkage.

Parameter	Value	Unit
Link l_{31}	206.53	[mm]
Link l_{32}	103.26	[mm]
Link l_3	103.26	[mm]
Link l_4	113.59	[mm]
Minimum stroke s_{min}	43.64	[mm]
Maximum stroke s_{max}	93.88	[mm]
Minimum input transmission angle $\mu_{3_{min}}$	24.61	[°]
Total height of the mechanism y_{max}	290.14	[mm]
Total size of the mechanism L_x	187.76	[mm]

The representation of the optimized seven-bar linkage $7-\underline{P}R(RRRR)R\underline{P}$ in the folded position and in the extended position is presented in Figure 10.

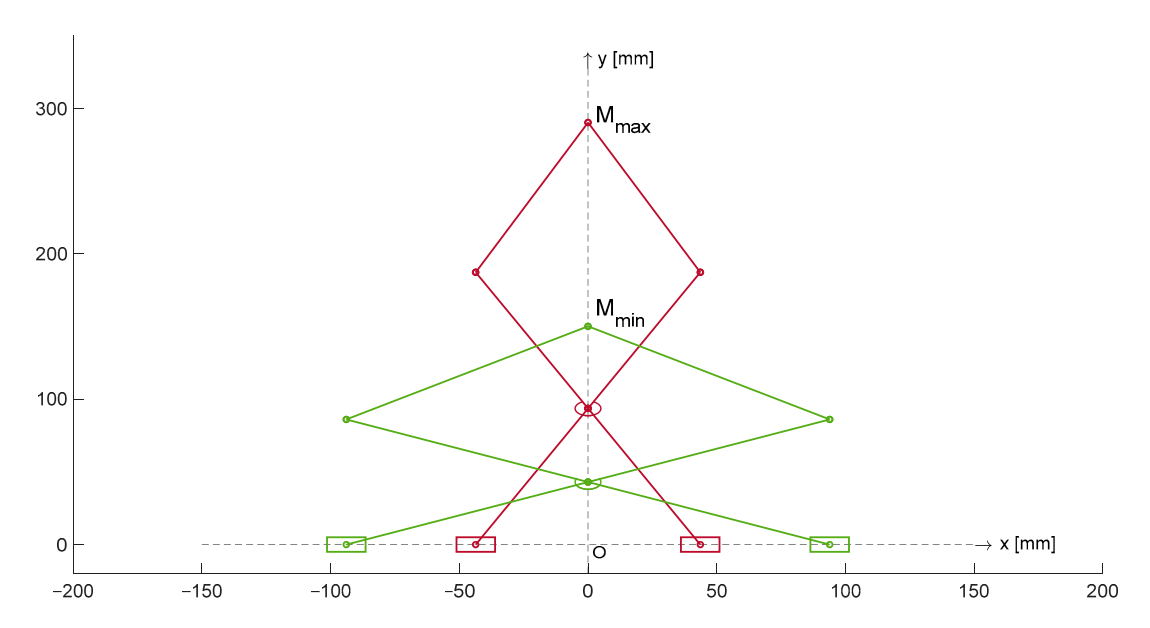


Figure 10. The optimized seven-bar linkage in its folded (green) and extended (red) position.

Robotics **2024**, 13, 177 17 of 24

6. Performance Analysis of the Optimized Seven-Bar Linkage 7-PR(RRRR)RP

6.1. Type I and Type II Singularities

First, in order to analyze the performance of the optimized seven-bar linkage 7- $\underline{P}R(RRR)R\underline{P}$, the Jacobian matrix determinants J_q and J_x must be determined:

$$det(J_q) = \begin{vmatrix} \frac{\partial F_3(X,Q)}{\partial s_3} & \frac{\partial F_3(X,Q)}{\partial s_6} \\ \frac{\partial F_6(X,Q)}{\partial s_6} & \frac{\partial F_6(X,Q)}{\partial s_6} \end{vmatrix} = 0$$
 (36)

$$det(J_x) = \begin{vmatrix} \frac{\partial F_3(X,Q)}{\partial x_M} & \frac{\partial F_3(X,Q)}{\partial y_M} \\ \frac{\partial F_6(X,Q)}{\partial x_M} & \frac{\partial F_6(X,Q)}{\partial y_M} \end{vmatrix} = 0$$
 (37)

where the transmission functions are as follows:

$$F_3(X,Q) = y_M^2 + s_3^2 + l_{31}^2 - l_4^2 - 2 \cdot s_3 \cdot l_{31} \cdot \cos \varphi_3 - 2 \cdot y_M \cdot l_{31} \cdot \sin \varphi_3 + x_M^2 + 2 \cdot x_M \cdot s_3 - 2 \cdot x_M \cdot l_{31} \cdot \cos \varphi_3$$
(38)

$$F_6(X,Q) = y_M^2 + s_6^2 + l_{61}^2 - l_5^2 + 2 \cdot s_6 \cdot l_{61} \cdot \cos \varphi_6 - 2 \cdot y_M \cdot l_{61} \cdot \sin \varphi_6 + x_M^2 - 2 \cdot x_M \cdot s_6 - 2 \cdot x_M \cdot l_{61} \cdot \cos \varphi_6$$
(39)

The vector of the input parameters of the seven-bar linkage is $Q = [s_3s_6]^T$ and the vector of the output parameters is $X = [x_My_M]^T$. In order to have a singularity-free workspace, both Jacobian matrix determinants J_q and J_x must have values different than zero so that both type I and type II singularities are avoided.

In order to have a better overview of the performance of the optimized seven-bar linkage, the next figures will also include the results for the other seven-bar linkages, obtained for the same optimal coefficient k = 1.1 and for the other values of the design coefficient p.

Figures 11 and 12 show that the singularities of type I and type II are avoided in the entire dexterous workspace, since no value of the Jacobian matrix determinant J_q nor J_x is zero. Still, the structures that are the closest to reach singularities positions are the ones computed with coefficient p = 0.75 and p = 1.25.

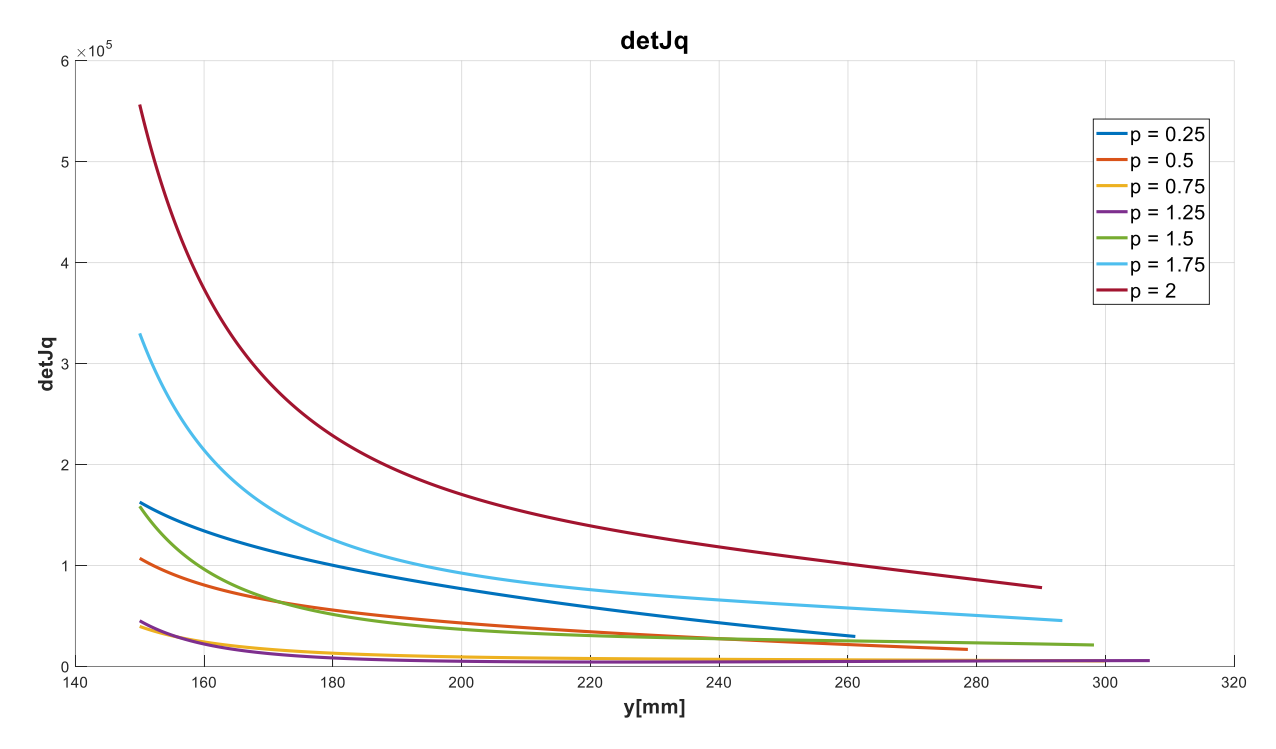


Figure 11. Type I singularities.

Robotics **2024**, 13, 177 18 of 24

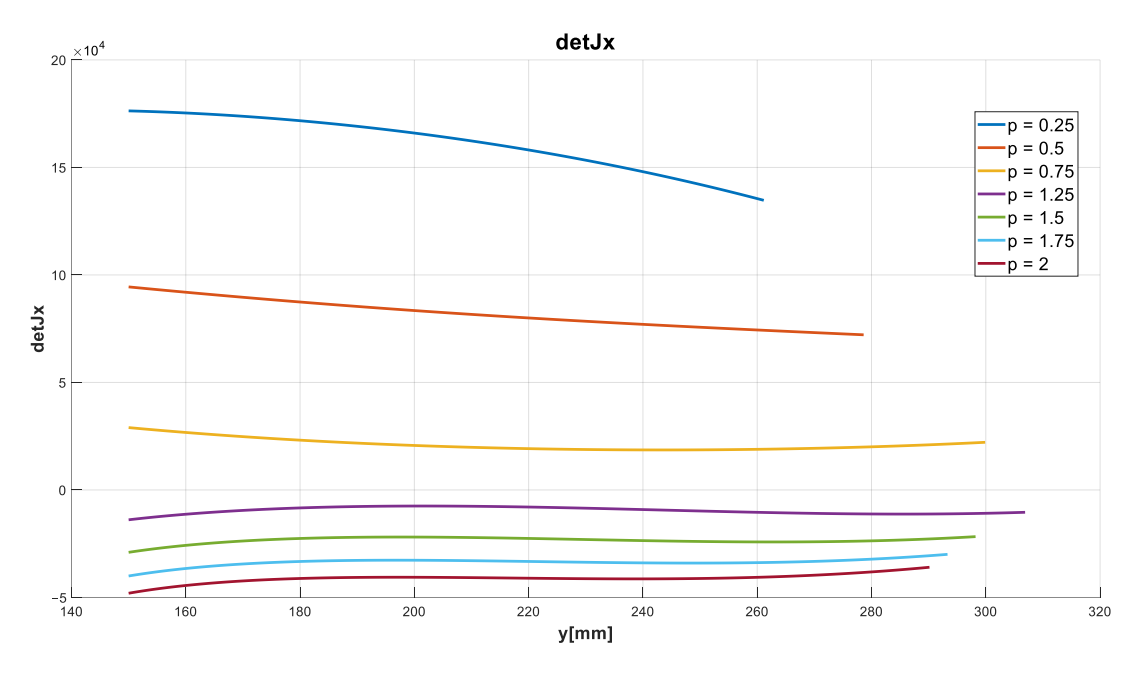


Figure 12. Type II singularities.

6.2. Local Manipulability Index (LMI) and Global Manipulability Index (GMI)

The first performance index [33] is the local manipulability index (*LMI*), which is defined as the absolute value of the Jacobian matrix determinant:

$$LMI = |\det J| = |\det \left(J_x J_q^{-1}\right)| \tag{40}$$

Figure 13 presents the values of the normalized local manipulability index, which were obtained by implementing the minimum-maximum normalization algorithm that rescaled the initial values in the range of [0; 1]. The values closer to 1 are considered to indicate a better maneuverability of the linkage.

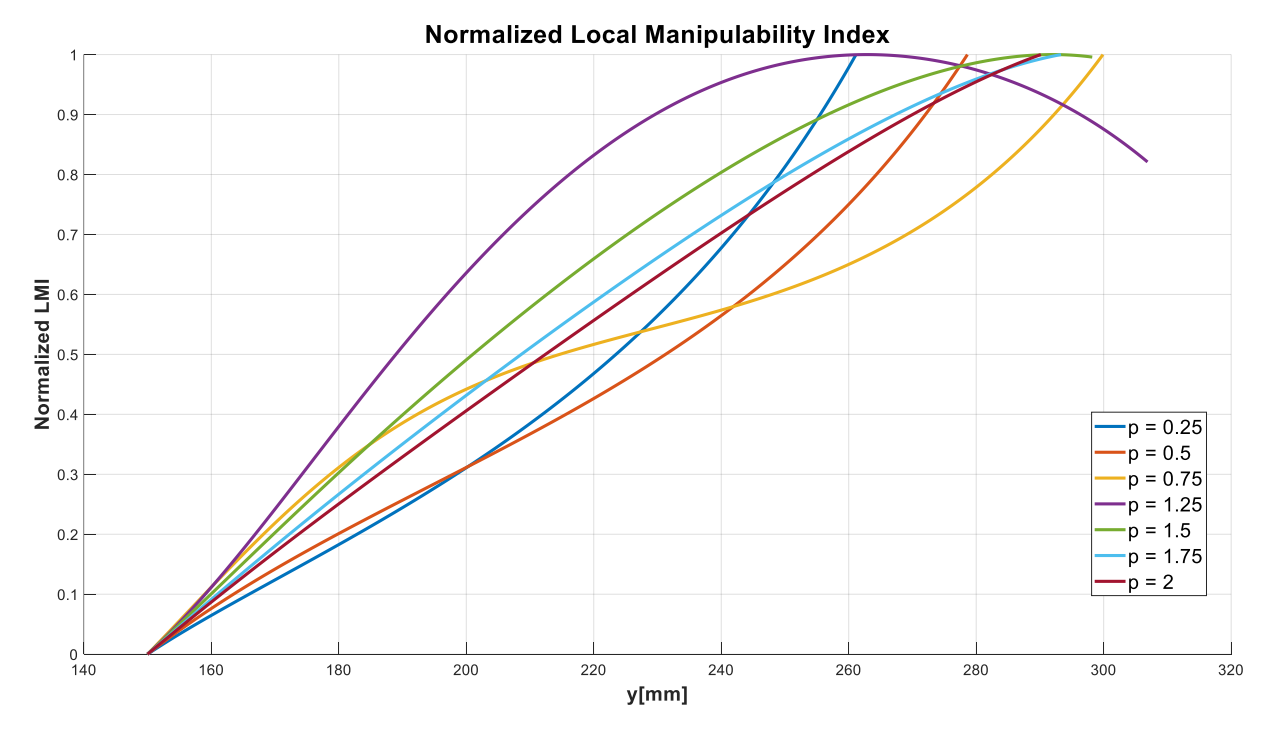


Figure 13. Normalized local manipulability index.

Robotics 2024, 13, 177 19 of 24

Furthermore, the global manipulability index (*GMI*) can be obtained by computing the local manipulability index (*LMI*) across the entire dexterous workspace W, according to the following equation:

$$GMI = \frac{\int_{w} \frac{1}{LMI} dw}{\int_{w} dw} \tag{41}$$

The global manipulability indexes for the optimized seven-bar linkage, computed with the coefficients k = 1.1 and p = 1, as well as for the other values of the design coefficient p, are given in Table 16.

Table 16. Global manipulability index (*GMI*).

	P	GMI
	0.25	0.3982
	0.5	0.4255
	0.75	0.5132
k = 1.1	1.25	0.7167
	1.5	0.6292
	1.75	0.5704
	2	0.5421

6.3. Condition Number, Local Condition Index (LCI) and Global Conditioning Index (GCI)

The next index is the condition number (CN), which is a measure of the degree of independence of the columns manipulator's Jacobian matrix [33] and is defined as the product between the absolute value of the Jacobian matrix determinant J and its inverse determinant:

$$CN = \|J\| \cdot \|J^{-1}\| \tag{42}$$

Due to the fact that the condition number (CN) takes values in the range of $[1, +\infty]$, it is more relevant to further consider the inverse values of the condition number (CN), known as the local condition index (LCI), which can be computed with the following relationship:

$$LCI = \frac{1}{CN} \tag{43}$$

The values of the local condition index (LCI), a kinematic performance measure, for the optimized seven-bar linkage, computed with the coefficients k = 1.1 and p = 1, as well as for the other values of the design coefficient p, are presented in Figure 14. An ideal value of LCI is considered to be closer to 1.

Furthermore, the global conditioning index (GCI) can be obtained by computing the local condition index (LCI) across the entire dexterous workspace W with the following relationship:

$$GCI = \frac{\int_{w} \frac{1}{CN} dw}{\int_{w} dw} \tag{44}$$

The values of the global conditioning indexes (GCI) for the optimized $\overline{2}$ -PR(RRRR)RP seven-bar linkage, computed with the coefficients k = 1.1 and p = 1, as well as for the other values of the design coefficient p, are given in Table 17. Similarly, better performance is associated with a GCI value closer to the ideal value of 1.

Robotics 2024, 13, 177 20 of 24

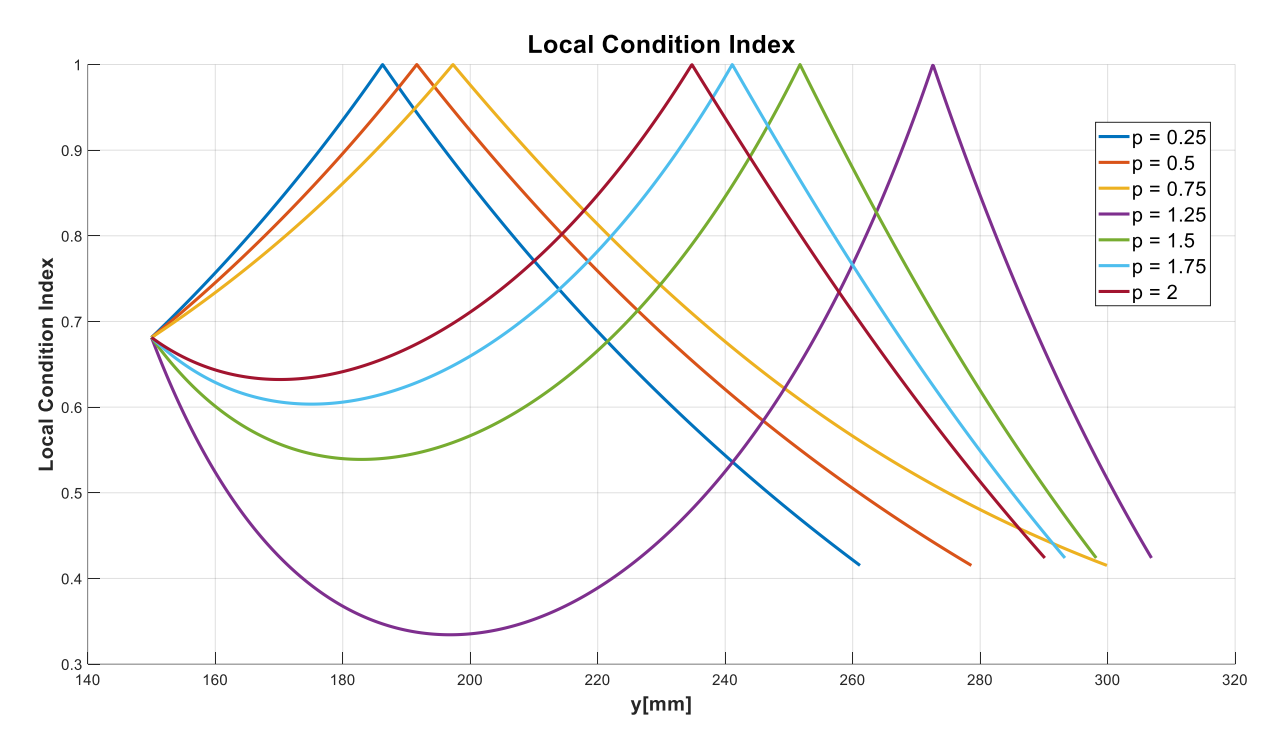


Figure 14. Local condition index (LCI).

Table 17. Global condition index (GCI).

	P	GCI
	0.25	0.7260
	0.5	0.7219
	0.75	0.7078
k = 1.1	1.25	0.5407
	1.5	0.6655
	1.75	0.7005
	2	0.7153

6.4. Kinematic Conditioning Index (KCI)

Another similar measure of the performance is the kinematic conditioning index (*KCI*), which is expressed in percentage and is computed with the following equation:

$$KCI = \frac{1}{CN_{min}} \cdot 100[\%] \tag{45}$$

The values of the kinematic conditioning indexes for the optimized seven-bar linkage, computed with the coefficients k = 1.1 and p = 1, as well as for the other values of the coefficient p, are given in Table 18.

Table 18. Kinematic conditioning index (*KCI*).

	P	KCI
	0.25	99.9911%
	0.5	99.9989%
	0.75	99.9955%
k = 1.1	1.25	99.9046%
	1.5	99.9976%
	1.75	99.9925%
	2	99.9753%

Robotics **2024**, 13, 177 21 of 24

Better performance of the 7-PR(RRRR)RP seven-bar linkage is once again associated with a kinematic conditioning index (*KCI*) value closer to 100%.

6.5. Local Stiffness Index (LSI)

The last performance index is the local stiffness index (*LSI*), which depends on multiple parameters such as the control system, the geometry, and the material of the elements, as well as on the actuators type [34], and can be computed with the following equation [35]:

$$LSI = K \cdot I^T \cdot I \tag{46}$$

where *K* is a scalar value (usually 1) that indicates each actuator's stiffness.

Figure 15 presents the local stiffness index (*LSI*) for the optimized seven-bar linkage, computed with the coefficients k = 1.1 and p = 1, as well as for the other values of the coefficient p.

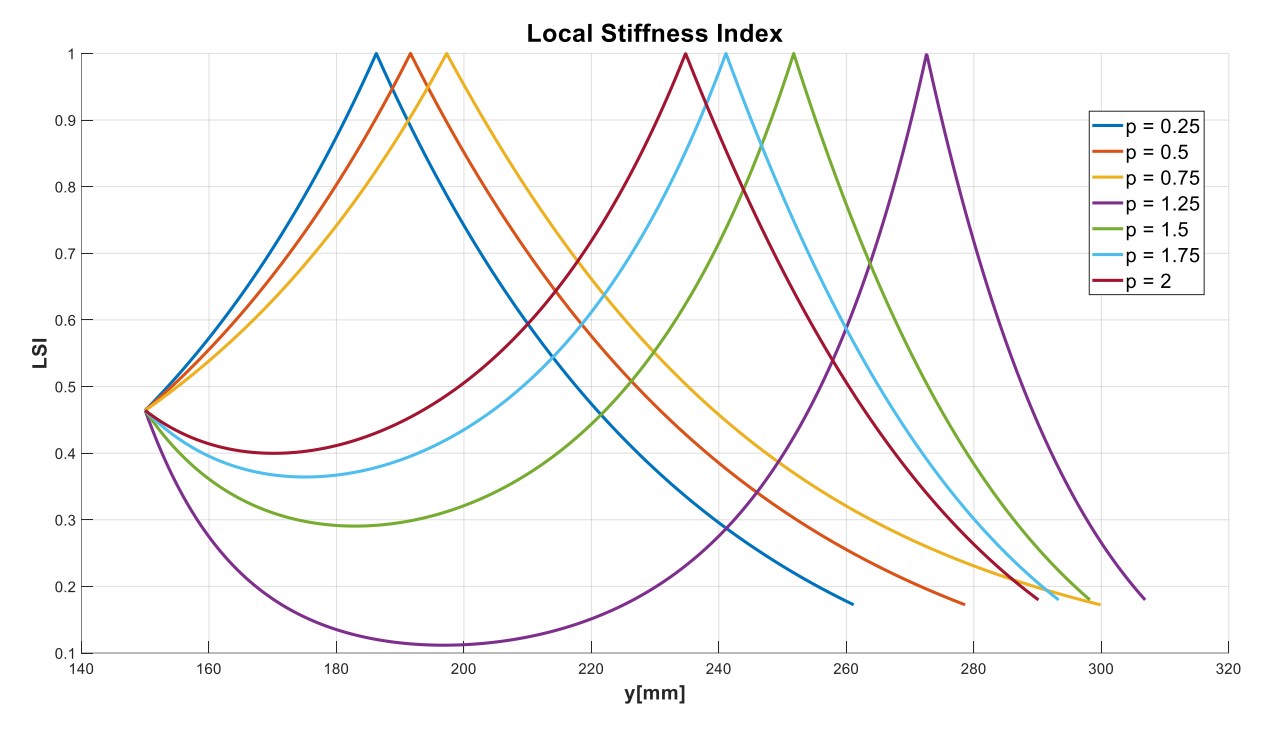


Figure 15. Local stiffness index (*LSI*).

7. Design of the Optimized Seven-Bar Linkage 7-PR(RRRR)RP and the Medical Disinfection Robot

Following the performance analysis, this chapter presents the design of the optimized seven-bar linkage 7-PR(RRRR) with the computed parameters.

Figure 16 presents the design of the medical disinfection robot in the folded position and in the extended position. The robot's structure consists of a mobile platform and two identical seven-bar linkages 7-PR(RRRR)RP which have four UV-C light sources mounted between them. The number of UV-C light sources, as well as their characteristics (e.g., diameter, length, wavelength, power), can be selected according to different types of requirements. For example, Philips offers a large variety of UV-C germicidal lamps for commercial or professional air, water, and surface disinfection, each one with their own key features and benefits. The mobile platform, with a size of $500 \times 500 \times 70$ mm, is driven by four mecanum wheels, each of them actuated independently by a stepper motor in order to allow the omnidirectional movement of the robot. Additionally, in order to also be able to perform floor disinfection, a large part of the mobile platform's bottom (250 \times 400 mm) is cut out. The movement of the medical disinfection robot's mechanism from the folded position (minimum configuration) to the extended position (maximum configuration) and

Robotics **2024**, 13, 177 22 of 24

vice versa is accomplished by a stepper motor through a scissor jack transmission type, with side guides for a better stability.

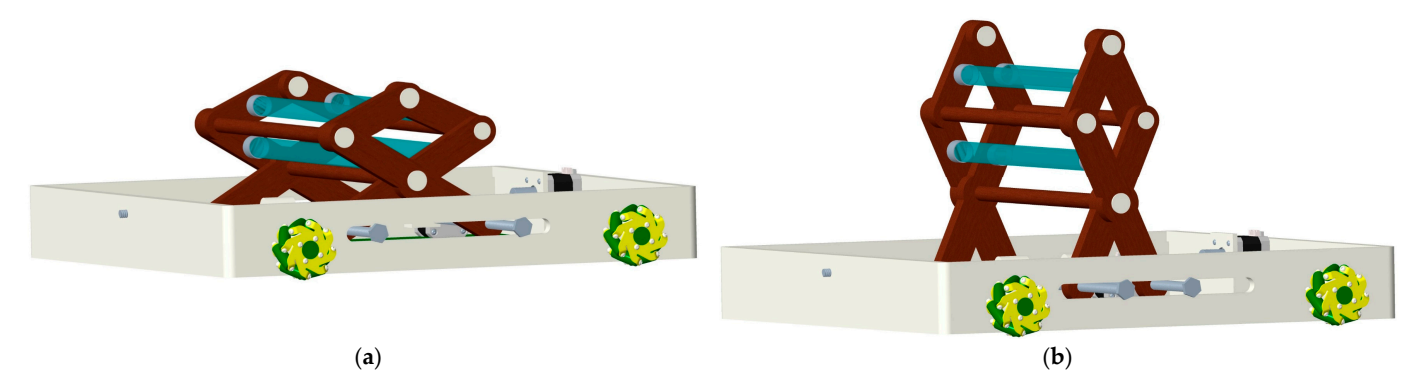


Figure 16. The medical disinfection robot. (a) Folded position; (b) extended position.

8. Conclusions

The article presented a feasibility study of the seven-bar linkage 7-PR(RRRR)RP used for the design of a medical disinfection robot with a folding mechanism. Since the current available disinfection robots cannot operate in small, tight, and narrow areas, the only solution to be able to effectively disinfect the hard-to-reach areas in medical facilities and other environments is to use medical disinfection robots with folding mechanisms. Their structure allows them to operate in multiple configurations based on the area type that needs to be disinfected, therefore ensuring the effectiveness of the sanitation process.

The initial parameters of the 7-PR(RRRR)RP seven-bar linkage were obtained as a result of a synthesis method from the inequalities system necessary in order to avoid the singularities positions of the mechanism. This method considered an arbitrary value of the coefficient k > 1, which was implemented to substitute the resulting inequalities system with an equation system, and different values of the design coefficient p. However, by applying this method, we could not be certain that the optimal 7-PR(RRRR)RP seven-bar linkage structure was obtained. Furthermore, an optimized synthesis method was applied, which considered the ratio between the total height and the total size of the mechanism. The parameters of the seven-bar linkage were computed for different values of the design coefficient $p \in [1.1; 2]$ and different values of the coefficient $k \in (0; 2]$. The optimal mechanism's kinematic design and structure was obtained by implementing a target function, which was computed using the normalized values of the total height and the total size of the mechanism, each of them having an imposed weight coefficient, c_1 and c_2 . The normalized values were obtained by implementing a minimum-maximum normalization algorithm that rescaled the initial values in the range of [0, 1], while the weight coefficients were both considered to be $c_1 = c_2 = 0.5$, which means that both the total height and the total size of the mechanism are considered equally important. Since the aim was to achieve the structure with the highest total height and the lowest total size, the target function needed to be maximized. Furthermore, the optimized seven-bar linkage 7-PR(RRRR)RP was computed with the parameters that resulted from the optimized synthesis method. The accuracy and the reliability of the results, as well as the feasibility of the design, are further strengthened by a performance analysis between the optimal indicated structure from the optimized synthesis method and other 7-PR(RRRR)RP seven-bar linkage structures, which were computed with different values of the parameters. Finally, the design of the medical disinfection robot with a folding mechanism showed its main advantages and its two main configurations, the folded position (minimum configuration) and the extended position (maximum configuration).

Future work includes building the medical disinfection robot, as well as performing experimental tests in order to establish the optimal mechanism's configuration, the UV-C disinfection source type (regarding the irradiance, power, and wavelength), and the optimal disinfection time and distance between the robot and the surfaces that need to be

Robotics 2024, 13, 177 23 of 24

disinfected in order to achieve the most effective disinfection process possible. Additionally, a mobile app will also be developed in order to be able to effectively control and navigate the medical disinfection robot through the disinfected environment.

Author Contributions: Conceptualization, E.-G.T. and E.-C.L.; methodology, E.-G.T. and E.-C.L.; software, E.-G.T., C.S. and A.O.; validation, E.-G.T., C.S. and E.-C.L.; formal analysis, E.-G.T.; investigation, E.-G.T. and E.-C.L.; resources, E.-G.T. and E.-C.L.; data curation, E.-G.T.; writing—original draft preparation, E.-G.T.; writing—review and editing, E.-G.T. and E.-C.L.; visualization, E.-G.T., C.S., A.O., M.O.S. and N.-G.C.; supervision, E.-C.L.; project administration, E.-C.L. All authors have read and agreed to the published version of the manuscript.

Funding: This research received no external funding.

Data Availability Statement: The original contributions presented in this study are included in the article. Further inquiries can be directed to the corresponding authors.

Acknowledgments: Special thanks go to Marco Ceccarelli for the support of this research.

Conflicts of Interest: The authors declare no conflicts of interest.

References

- 1. Mehta, I.; Hsueh, H.-Y.; Taghipour, S.; Li, W.; Saeedi, S. UV Disinfection Robots: A Review. *Robot. Auton. Syst.* **2023**, *161*, 104332. [CrossRef] [PubMed]
- Diab-El Schahawi, M.; Zingg, W.; Vos, M.; Humphreys, H.; Lopez-Cerero, L.; Fueszl, A.; Zahar, J.R.; Presterl, E. Ultraviolet disinfection robots to improve hospital cleaning: Real promise or just a gimmick? *Antimicrob. Resist. Infect. Control* 2021, 10, 33.
 [CrossRef] [PubMed]
- 3. Bratu, D.-V.; Zolya, M.-A.; Moraru, S.-A. RoboCoV Cleaner: An Indoor Autonomous UV-C Disinfection Robot with Advanced Dual-Safety Systems. *Sensors* **2024**, *24*, 974. [CrossRef] [PubMed]
- 4. Wang, S.; Li, Y.; Ding, G.; Li, C.; Zhao, Q.; Sun, B.; Song, Q. Design of UVC Surface Disinfection Robot with Coverage Path Planning Using Map-Based Approach At-The-Edge. *Robotics* **2022**, *11*, 117. [CrossRef]
- 5. Xu, P.; Chen, X.; Tang, Q. Design and Coverage Path Planning of a Disinfection Robot. Actuators 2023, 12, 182. [CrossRef]
- 6. Wang, N.; Shi, C.; Kang, X. Design of a Disinfection and Epidemic Prevention Robot Based on Fuzzy QFD and the ARIZ Algorithm. *Sustainability* **2022**, *14*, 16341. [CrossRef]
- 7. Ramalingam, B.; Yin, J.; Rajesh Elara, M.; Tamilselvam, Y.K.; Mohan Rayguru, M.; Muthugala, M.A.V.J.; Félix Gómez, B. A Human Support Robot for the Cleaning and Maintenance of Door Handles Using a Deep-Learning Framework. *Sensors* **2020**, 20, 3543. [CrossRef]
- 8. Van, T.N.; Xuan, N.H.; Duc, N.N. Design and development of multifunctional autonomous mobile disinfection robot against SARS-CoV-2 virus. *Int. J. Mech. Eng. Robot. Res.* **2022**, *11*, 718–723. [CrossRef]
- 9. Sang, A.W.Y.; Moo, C.G.; Samarakoon, S.M.B.P.; Muthugala, M.A.V.J.; Elara, M.R. Design of a Reconfigurable Wall Disinfection Robot. *Sensors* **2021**, *21*, 6096. [CrossRef]
- 10. Chen, C.-S.; Lin, F.-C.; Lin, C.-J. The Energy Efficiency Multi-Robot System and Disinfection Service Robot Development in Large-Scale Complex Environment. *Sensors* **2023**, 23, 5724. [CrossRef]
- 11. Yao, Z.; Ma, N.; Chen, Y. An Autonomous Mobile Combination Disinfection System. Sensors 2024, 24, 53. [CrossRef] [PubMed]
- 12. Kunz Cechinel, A.; Soares, C.E.; Pfleger, S.G.; De Oliveira, L.L.G.A.; Américo de Andrade, E.; Damo Bertoli, C.; De Rolt, C.R.; De Pieri, E.R.; Plentz, P.D.M.; Röning, J. Mobile Robot + IoT: Project of Sustainable Technology for Sanitizing Broiler Poultry Litter. *Sensors* 2024, 24, 3049. [CrossRef] [PubMed]
- 13. Tulcan, E.-G.; Oarcea, A.; Lovasz, E.-C. Analytical Synthesis of the Seven-Bar Linkage 7-RR(RRR)R used for Medical Disinfection Robot. In *Mechanisms and Machine Science, Proceedings of the 2nd International Workshop IFToMM for Sustainable Development Goals (I4SDG), Bilbao, Spain, 22–23 June 2023*; Petuya, V., Quaglia, G., Parikyan, T., Carbone, G., Eds.; Springer: Cham, Switzerland, 2023; Volume 134, pp. 171–180. [CrossRef]
- 14. Tulcan, E.-G.; Sticlaru, C.; Oarcea, A.; Sandu, M.O.; Lovasz, E.-C. Kinematic Analysis of the Seven-Bar Linkage 7-PR(RRRR)RP Used for Medical Disinfection Robot. In *Mechanisms and Machine Science, Proceedings of the 33rd International Conference on Robotics in Alpe-Adria Danube Region (RAAD), Cluj-Napoca, Romania, 5–7 June 2024*; Pisla, D., Carbone, G., Condurache, D., Vaida, C., Eds.; Springer: Cham, Switzerland, 2024; Volume 157, pp. 359–367. [CrossRef]
- 15. Tulcan, E.G.; Oarcea, A.; Sticlaru, C.; Ceccarelli, M.; Lovasz, E.C. Analytical Synthesis of the Seven-Bar Linkage 7-PR(RRRR)RP Used for Medical Disinfection Robot. In *Mechanisms and Machine Science, Proceedings of the 6th IFToMM Symposium on Mechanism Design for Robotics (MEDER), Timiṣoara, Romania, 27–29 June 2024*; Lovasz, E.C., Ceccarelli, M., Ciupe, V., Eds.; Springer: Cham, Switzerland, 2024; Volume 166, pp. 334–344. [CrossRef]

Robotics 2024, 13, 177 24 of 24

16. Tulcan, E.G.; Sticlaru, C.; Lovasz, E.C. Design of a Medical Robot with Folding Mechanism Used for Disinfection in the Hard-to-Reach Areas. In *Mechanisms and Machine Science, Proceedings of the International Workshop on Medical and Service Robots (MEDER), Craiova, Romania, 5–7 June* 2023; Tarnita, D., Dumitru, N., Pisla, D., Carbone, G., Geonea, I., Eds.; Springer: Cham, Switzerland, 2023; Volume 133, pp. 351–359. [CrossRef]

- 17. Tivadar, D.; Oarcea, A.; Ceccarelli, M.; Lovasz, E.C.; Buncianu, D.; Silaghi-Perju, D.C. Analytical Synthesis of Five-Bar Linkage 5-PRRP. In *Mechanisms and Machine Science, Proceedings of the IFToMM World Congress on Mechanism and Machine Science, Tokyo, Japan, 5–10 November* 2023; Okada, M., Ed.; Springer: Cham, Switzerland, 2023; Volume 149, pp. 321–331. [CrossRef]
- 18. Tulcan, E.-G.; Sticlaru, C.; Oarcea, A.; Lovasz, E.-C. Medical Disinfection Robots: Past vs. Future. Improving the Disinfection Process by Using Disinfection Robots with Folding Mechanism. In Proceedings of the 17th International Conference on Engineering of Modern Electric Systems, Oradea, Romania, 9–10 June 2023. [CrossRef]
- 19. Zaman, A.; Majib, M.S.; Tanjim, S.A.; Siddique, S.M.A.; Islam, S.; Aadeeb, M.S.; Khan, N.I.; Haque, R.; Islam, M.R.U.; Faisal, M.R.F.; et al. UVC-PURGE. A novel cost-effective robot. *IEEE Access* 2022, 10, 37613–37634. [CrossRef] [PubMed]
- 20. Sedaghat, M.; Madani, P.; Alvari, Y.; Jahangiri, A. Studying the effect of a disinfection robot using UVC lights, on fungi and microbes in the hospital environment. In Proceedings of the 10th RSI International Conference on Robotics and Mechatronics (ICRoM), Tehran, Iran, 22–24 November 2022. [CrossRef]
- 21. Chaari, M.Z.; Abdelfath, M.; Loreono, C.; Al-Rahimi, R. UV-C disinfection robotic. In Proceedings of the International Electronics Symposium (IES), Surabaya, Indonesia, 9–11 August 2022; pp. 336–342. [CrossRef]
- 22. Ruan, K.; Wu, Z.; Xu, Q. Smart Cleaner: A New Autonomous Indoor Disinfection Robot for Combating the COVID-19 Pandemic. *Robotics* **2021**, *10*, 87. [CrossRef]
- 23. Megalingam, R.K.; Raj, A.; Manoharan, S.K.; Egumadiri, E. App based teleoperated UV disinfectant robot for Covid cause. In Proceedings of the 2nd International Conference on Electronics and Sustainable Communication Systems (ICESC), Coimbatore, India, 4–6 August 2021; pp. 277–281. [CrossRef]
- 24. Füszl, A.; Zatorska, B.; Van den Nest, M.; Ebner, J.; Presterl, E.; Diab-Elschahawi, M. The use of a UV-C disinfection robot in the routine cleaning process: A field study in an Academic hospital. *Antimicrob. Resist. Infect. Control* **2021**, *10*, 84. [CrossRef]
- 25. Reque, A.M.; Garay, E.F.; Cornejo, J.; Palomares, R. Mechatronics design and kinematic analysis of mecanum wheeled mobile robot for COVID-19 disinfection with UV rays applied on indoor environments. In Proceedings of the IEEE Sciences and Humanities International Research Conference (SHIRCON), Lima, Peru, 17–19 November 2021; pp. 1–4. [CrossRef]
- 26. Camacho, E.C.; Ospina, N.I.; Calderón, J.M. COVID-Bot: UV-C Based Autonomous Sanitizing Robotic Platform for COVID-19. *IFAC-Papersonline* **2021**, *54*, 317–322. [CrossRef]
- 27. Mohan, A.; Krishnan, A.R. Design and Simulation of an Autonomous Floor Cleaning Robot with Optional UV Sterilization. In Proceedings of the 2nd Mysore Sub Section International Conference (MysuruCon), Mysuru, India, 16–17 October 2022; pp. 1–6. [CrossRef]
- 28. Conroy, J.; Thierauf, C.; Rule, P.; Krause, E.; Akitaya, H.; Gonczi, A.; Korman, M.; Scheutz, M. Robot Development and Path Planning for Indoor Ultraviolet Light Disinfection. In Proceedings of the IEEE International Conference on Robotics and Automation (ICRA), Xi'an, China, 30 May–5 June 2021; pp. 7795–7801. [CrossRef]
- 29. McGinn, C.; Scott, R.; Donnelly, N.; Roberts, K.; Bogue, M.; Kiernan, C.; Beckett, M. Exploring the applicability of robot-assisted UV disinfection in radiology. *Front. Robot. AI* **2021**, *7*, 590306. [CrossRef]
- 30. Zhao, Y.; Huang, H.; Chen, T.; Chiang, P.; Chen, Y.; Yeh, J.; Huang, C.; Lin, J.; Weng, W. A Smart Sterilization Robot System with Chlorine Dioxide for Spray Disinfection. *IEEE Sens. J.* **2021**, 21, 22047–22057. [CrossRef]
- 31. Mehta, A.; Apeksha, S.; Banagar, P. Design, Analysis and Development of an Autonomous Modular Disinfectant Robot. In Proceedings of the IEEE International Conference on Electronics, Computing and Communication Technologies (CONECCT), Bangalore, India, 8–10 July 2022; pp. 1–6. [CrossRef]
- 32. Song, L.; Li, W.; He, J.; Li, L.; Li, T.; Gu, D.; Tang, H. Development of pulsed xenon ultraviolet disinfection device for real-time air disinfection in ambulances. *J. Healthc. Eng.* **2020**, 2020, 6053065. [CrossRef] [PubMed]
- 33. Patel, S.; Sobh, T. Manipulator Performance Measures—A Comprehensive Literature Survey. *J. Intell. Robot. Syst.* **2015**, 77, 547–570. [CrossRef]
- 34. Luputi, A.-M.-F.; Lovasz, E.-C.; Ceccarelli, M.; Sticlaru, C.; Scurt, A.-M. Kinematic study of feasibility of geared planar parallel manipulator. *Proc. Inst. Mech. Eng. Part C J. Mech. Eng. Sci.* **2022**, 236, 10001–10016. [CrossRef]
- 35. Lee, K.M.; Johnson, R. Static characteristics of an in-parallel actuated manipulator for clamping and bracing applications. In Proceedings of the 1989 International Conference on Robotics and Automation, Scottsdale, AZ, USA, 14–19 May 1989; pp. 1408–1413. [CrossRef]

Disclaimer/Publisher's Note: The statements, opinions and data contained in all publications are solely those of the individual author(s) and contributor(s) and not of MDPI and/or the editor(s). MDPI and/or the editor(s) disclaim responsibility for any injury to people or property resulting from any ideas, methods, instructions or products referred to in the content.